Journal of Energy Chemistry 80 (2023) 689–710

Contents lists available at ScienceDirect

Journal of Energy Chemistry

journal homepage: www.elsevier.com/locate/jechem

http://www.journals.elsevier.com/journal-of-energy-chemistry/

Review

Solvent engineering towards scalable fabrication of high-quality perovskite films for efficient solar modules

Zhaoyi Jiang [a,1], Binkai Wang [a,b,1], Wenjun Zhang [a,1], Zhichun Yang [c,d,*], Mengjie Li [e], Fumeng Ren [a], Tahir Imran [a], Zhenxing Sun [a], Shasha Zhang [f], Yiqiang Zhang [f], Zhiguo Zhao [e,*], Zonghao Liu [a,*], Wei Chen [a,*]

[a] Wuhan National Laboratory for Optoelectronics (WNLO), Huazhong University of Science and Technology (HUST), Wuhan 430074, Hubei, China
[b] China-EU Institute for Clean and Renewable Energy (ICARE), Huazhong University of Science and Technology (HUST), Wuhan 430074, Hubei, China
[c] State Key Lab of Quantum Optics and Quantum Optics Devices, Institute of Laser Spectroscopy, Shanxi University, Taiyuan 030006, Shanxi, China
[d] Collaborative Innovation Center of Extreme Optics, Shanxi University, Taiyuan 030006, Shanxi, China
[e] Huaneng Clean Energy Research Institute, Beijing, China
[f] School of Materials Science and Engineering & Henan Institute of Advanced Technology, Zhengzhou University, Zhengzhou 450001, Henan, China

ARTICLE INFO

Article history:
Received 2 December 2022
Revised 28 January 2023
Accepted 2 February 2023
Available online 17 February 2023

Keywords:
Solvent engineering
Scalable fabrication
Perovskite film
Solar cell
Module

ABSTRACT

Over the last decade, remarkable progress has been made in metal halide perovskite solar cells (PSCs), which have been a focus of emerging photovoltaic techniques and show great potential for commercialization. However, the upscaling of small-area PSCs to large-area solar modules to meet the demands of practical applications remains a significant challenge. The scalable production of high-quality perovskite films by a simple, reproducible process is crucial for resolving this issue. Furthermore, the crystallization behavior in the solution-processed fabrication of perovskite films can be strongly influenced by the physicochemical properties of the precursor inks, which are significantly affected by the employed solvents and their interactions with the solutes. Thus, a comprehensive understanding of solvent engineering for fabricating perovskite films over large areas is urgently required. In this paper, we first analyze the role of solvents in the solution-processed fabrication of large-area perovskite films based on the classical crystal nucleation and growth mechanism. Recent efforts in solvent engineering to improve the quality of perovskite films for solar modules are discussed. Finally, the basic principles and future challenges of solvent system design for scalable fabrication of high-quality perovskite films for efficient solar modules are proposed.

Contents

* Corresponding authors.
E-mail addresses: yangzhichun@sxu.edu.cn (Z. Yang), zg_zhao@qny.chng.com.cn (Z. Zhao), liuzonghao@hust.edu.cn (Z. Liu), wnlochenwei@mail.hust.edu.cn (W. Chen).
[1] These authors contributed equally to this work.

https://doi.org/10.1016/j.jechem.2023.02.017

1. Introduction

Capturing clean and renewable energy has been put forth as a practical approach to address the accelerating global energy crisis and increases in environmental pollution. Photovoltaic (PV) technology, which can efficiently harvest solar energy, stands out among various new energy technologies because it has a high performance and is environmentally friendly [1–8]. Solar cells based on metal halide perovskite light absorbers have been of interest in the last decade because of their remarkable device performance and cost-effective manufacturing process [9–12]. To date, the highest power conversion efficiency (PCE) of small-area perovskite solar cells (PSCs) has reached 25.7%, approaching the record efficiency of crystalline silicon (c-Si) solar cells, and the operational stability of PSCs has dramatically improved since 2009 [13,14]. Subsequently, reliable and scalable approaches for fabricating large-area devices are needed to integrate solar panels and move this emerging PV technology towards commercialization.

Perovskite solar modules (PSMs) can enhance the output voltage or current when they are scribed with a laser or mechanical knife into numerous sub-cells; they are then interconnected with suitable conductors to fulfill practical power demands. Therefore, PSM interconnection types can be classified as series or parallel types. In addition, PSMs can be classified into mini-modules, sub-modules, and modules based on the device area [15]. In general, an inevitable efficiency loss occurs as the device area increases. In addition, the decline rate is usually approximately 0.8% of the absolute efficiency, while the device area increases by one magnitude in commercially mature technologies (Fig. 1a). Currently, the highest efficiency of PSCs dramatically decreased to 23.7%, 21.4%, and 18.2% for standard 1 cm^2 cells, mini-modules (19.32 cm^2), and sub-modules (756 cm^2), respectively [16,17]. Therefore, the average decline in efficiency for current PSCs is 2%–3% of the absolute value as the device area increases by one magnitude, which is much higher than the general decline. This significant difference indicates a tremendous challenge in the scalable fabrication of PSMs. The inherent reasons for these differences can be ascribed to the following causes: (1) the quality of large-area functional layers (especially for perovskite layer) cannot catch up with their counterparts in small-area devices and have higher defect densities, more pinholes, and less uniformity in morphology and thickness; (2) laser/mechanical scribing induces dead region/heat-damaged regions around the active films and contact resistance losses at interconnection channels; and (3) the increase in the sheet resistance of the transparent conductive oxide (TCO) substrate that occurs as the device area increases.

In this context, we mainly focus on the upscaling fabrication of high-quality perovskite films for solar modules [18–25]. The quality of the perovskite film is known to play a decisive role in the generation and transportation of photogenerated carriers and the performance of PSCs and PSMs. Thus, achieving high-quality perovskite films over a large area by spin-coating coupled with the antisolvent extraction method for small-area PSCs remains a significant challenge. In particular, the uniformity of large-area perovskite films must be ensured, while the performance of PSMs is limited by the worst sub-cell [26–29]. Therefore, a manufacturing procedure of large-area perovskite films for PSMs using a simple and reproducible technique with less dependence on the atmosphere is urgently desired to replace the preparation of small-area devices using standard spin-coating methods in Ar- or N_2-filled gloveboxes. Recently, various deposition techniques have been developed, which are mainly divided into the dry method (mainly for chemical vapour deposition and evaporation deposition, as shown in Table 1 and Fig. 1b) and wet (solution) processing [16,22,30–43].

In contrast to the dry method, the solution-processed method allows high-throughput manufacturing and precise control of the stoichiometric ratio of the perovskite film. This article mainly discusses the progress of solvent engineering in the solution-processed fabrication of large-area perovskite films to manufacture efficient solar modules, including techniques such as spray coating, blade coating, slot-die coating, and inkjet printing, and

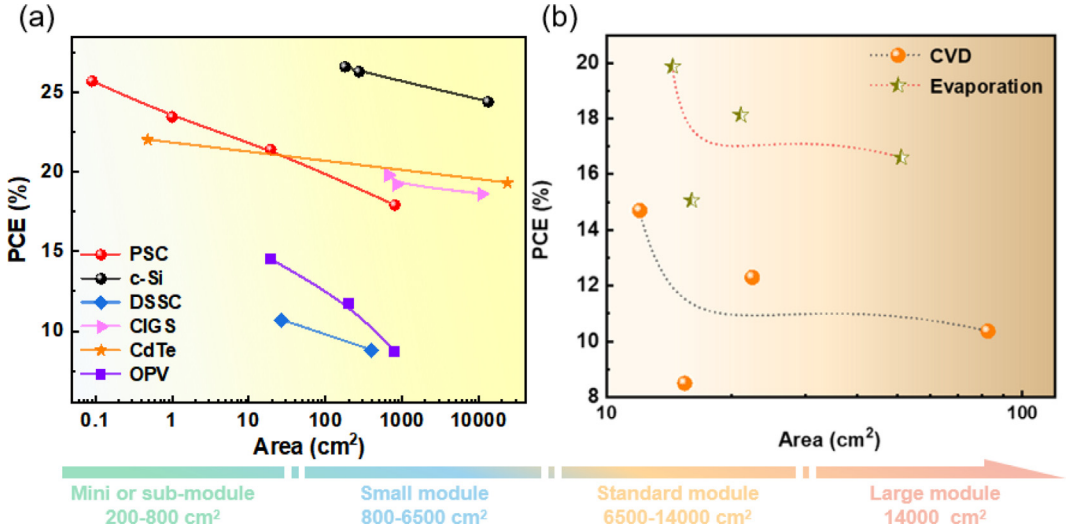

Fig. 1. (a) The power conversion efficiency evolution of various solar cells with different device areas. (b) The power conversion efficiency evolution of solar cells prepared by the dry methods.

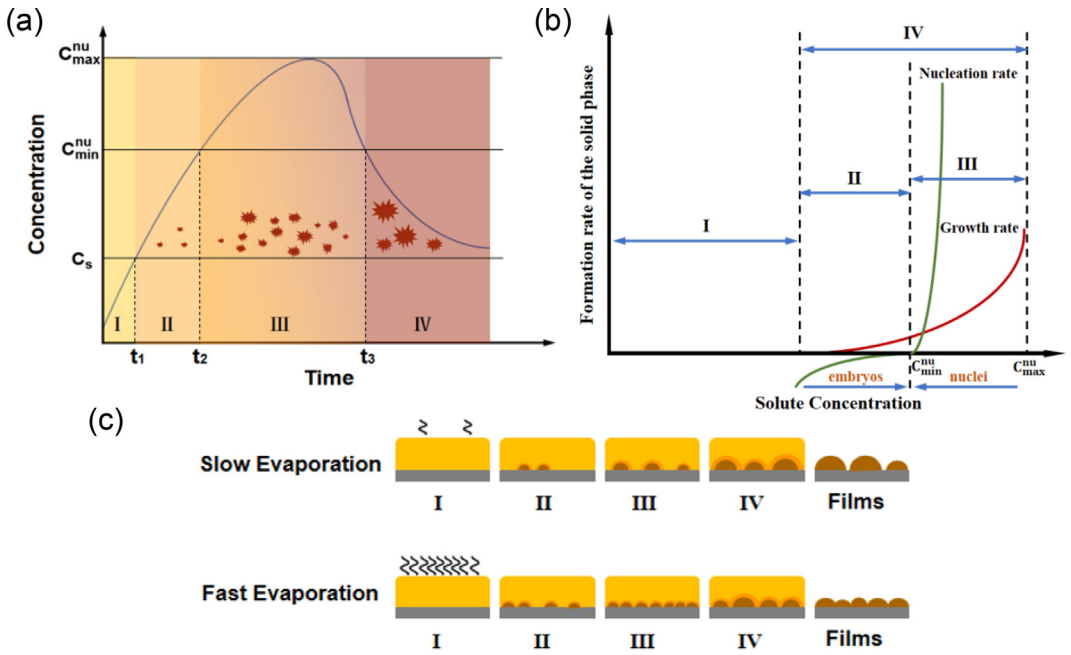

Fig. 2. (a) The changes of concentration as a function of time with solvents evaporating. (b) Schematic illustrating the nucleation and growth rates with solvents evaporating. Reproduced with permission from Ref. [68]. Copyright 2017, Royal Society of Chemistry. (c) The nucleation theory: the behaviors in solvent evaporation. Reproduced with permission from Ref. [34]. Copyright 2019, Royal Society of Chemistry.

provides a summary of the performance of PSMs (Table 2) fabricated using these methods [44–67].

Fundamentally, solvent engineering for various solution-processed fabrication processes of perovskite films precisely manipulates crystal growth dynamics. In general, the growth process of crystals is subject to the classical LaMer Model, schematically illustrated in Fig. 2(a) [68]. First, with the evaporation of the solvents, the concentration of the precursor solute gradually reaches saturation (C_s) after the precursor ink spreads on the target substrate, as illustrated in Fig. 2(a) (process I), coupled with the upcoming formation of embryos. As the solvents continually evaporate, the concentration of solute reaches the minimum for nucleation (C_{min}^{nu}); the nucleation behaviour starts at this point (Fig. 2b, process II) and the Gibbs free energy is higher than the surface energy of the formed nuclei from this point. In other words, this process can be understood as the growth of embryos towards the nucleus. During this period (from process I to process II in Fig. 2a and b), the embryos formed to overcome the critical nuclear barrier and grow to the critical nucleation radius (Fig. 2b, process II), which is also why nucleation cannot occur at C_s. Second, a coexistence process occurs, which includes the formation of the nucleus and the growth process (process III in Fig. 2b), during which the included atoms, ions, or molecules in the spread precursor ink are assembled to form new embryos or nuclei, and the maximum solute concentration is reached (C_{nu}^{max}). Finally, the solute concentration gradually decreases as the solute is consumed and only the nucleus growth process remains (process IV in Fig. 2a). The crystal growth rate is very fast once the nucleus is formed (process III in Fig. 2b).

Consequently, the key to manipulating the nucleation and growth kinetics is to control the volatilization rate of the solvents (as illustrated in Fig. 2c) used in the prepared precursor ink. In addition, nucleation and growth kinetics are also determined by the properties of the solvents, such as their volatility, boiling point, polarity, and interactions with the precursors [34,69–73]. In addition, these properties also affect the design of post-treatment strategies for the scalable fabrication of films. In addition, the nucleation density (N) in the precursor films can be estimated by the nucleation factor (P) and probability of atomic diffusion (Γ) according to formula (1); these values are affected by the solution viscosity (η), initial solution concentration (C_0), and critical energy barrier (ΔG^*) [68].

$$N = P\Gamma = \left\{\frac{C_0 KT}{3\pi\lambda^3\eta}\right\}\exp\left(\frac{-\Delta G^*}{KT}\right) \quad (1)$$

The C_0 value of the precursor inks is generally controlled by the solvent evaporation rate, which can be tailored by the solvent boiling point or extraction method. However, η or ΔG^* is significant for the diffusion and incorporation of atoms/ions into a liquid–solid interface in precursor inks. Hence, the influence of solvents adopted in the precursor inks is crucial to achieving a scalable fabrication process. In contrast to small-area PSCs, the photovoltaic characteristics of every subcell have an essential impact on the overall performance of the series of structural perovskite thin-film modules. Hence, uniformity of perovskite films over a large area is necessary for efficient PSMs. In addition, because of the non-uniform hydrophilicity of the substrates and solvents-extraction, the growth process of perovskite crystals during scalable fabrication of perovskite films is complicated and uncontrollable, resulting in the "Coffee Ring Effect". Therefore, to achieve a scalable fabrication process, an optimized solvent system should ensure a sufficient time window for wet film and controllable solvent extraction to improve the uniformity and crystallization quality of the film over a large area.

We first examined the basic roles and design principles of solvents in perovskite precursor inks, how they affect the quality of large-area perovskite films and the performance evolution of PSMs. Second, recent efforts in solvent engineering, as well as reasonable post-operation strategies for efficient PSMs, are systematically reviewed. Finally, perspectives for the further optimization of green solvent engineering design strategies aimed at creating perovskite films for highly efficient PSMs are provided to promote their commercialization.

2. The basic roles of solvents in perovskite crystallization

Tremendous efforts have been devoted to the solution-processed fabrication of uniform perovskite films over a large area by implementing solvent engineering with appropriate solvent and additive combinations [74,75]. There are three primary types of solvent systems used for the large-scale deposition of perovskite films: highly volatile, non-coordinating chemical solvents (VNCS); moderately volatile, coordinating chemical solvents (MVCS); and particularly less volatile, strongly chelating Lewis base additions (SCLA) [76–78]. As a result, their relative amounts can significantly affect the solvent evaporation rate and crystallization kinetics, which have far-reaching effects on the final perovskite film morphology. In general, the boiling points or vapor pressures of solvents and their coordination with Pb^{2+} or monovalent cations in precursor inks are critical for controlling the growth process of crystals [79]. For instance, VNCS such as acetonitrile (ACN) and 2-methoxy ethanol (2-ME) are easily removed from precursor inks because of their comparatively weak coordination with Pb^{2+} or monovalent cations.

In contrast, extracting solvents with relatively high boiling points and strong coordination is difficult [67,80,81]. The solvent ratio in the precursor inks determines the post-extraction strategies used in the preparation of the perovskite films. To produce a full-coverage morphology free of pinholes during the drying process of perovskite films, the rapid removal of the VNCS can induce supersaturation within a short time. In addition, owing to their higher boiling point and stronger coordination ability, MVCS solvents are required to enhance the solubility of perovskite chemicals. Several Lewis bases have been widely used to control this process by forming a stable intermediate phase [82,83]. However, several desired perovskite compositions cannot be processed without MVCS, resulting in a short lifetime of photogenerated carriers without SCLA. Thus, the combination of VNCS, MVCS, and SCLA at appropriate ratios to precisely adjust the physical and chemical properties of the mixed precursor is crucial for up-scaling the fabrication of perovskite films, as depicted in Fig. 3.

In addition to the self-evaporation of solvents in wet films, the supersaturation of precursor inks can be regulated by relevant post-treatments. To date, various post-treatments, including substrate heating, the vacuum flash method, gas knife blowing, and antisolvent bath, have been designed for fabricating large-scale perovskite films. However, further optimization is still required to achieve high homogeneity and reproducibility. Antisolvent removal is a common and well-established post-treatment method for preparing perovskite films in laboratories. This process consumes many chemical reagents for large-scale fabrication and may not be a cost-effective and environmentally friendly strategy [84,85]. Consequently, heating the substrate, vacuum flash, and gas knife-assisted coating methods have been developed in recent years. In summary, to achieve a controllable process, rapidly removing solvents and forming a stable intermediate phase from precursor states by adjusting the composition of the solvent system, or their physical or chemical properties, are key.

Precursor inks can be coated onto the prepared substrates using spin-coating techniques in a laboratory. The wet films can then be transformed into solid films by post-treatment, similar to the commonly used antisolvent extraction method. As shown in Fig. 4(a), the reagent for antisolvent extraction should be miscible with MVCS and SCLA in precursor inks, but insoluble in their solutes. When fabricating large-area perovskite films, antisolvents such as ethyl acetate (EA), chlorobenzene (CB), and diethyl ether (DEE) are often utilized as either drop-on treatments or soak solutions in extraction baths. Once the antisolvent is applied, solvents such as *N*, *N*-dimethylformamide (DMF), and dimethyl sulfoxide (DMSO) are efficiently eliminated from the wet state, leaving behind the perovskite crystals and intermediate phase in the prepared films [86]. DMSO in the intermediate phase was removed entirely in the subsequent annealing process.

In addition, by introducing VNCS into the prepared precursor inks, such as 2-ME and ACN, the solvent removal rate can be accelerated, which facilitates the quick removal of VNCS in wet films by gas knife flow. During the drying process, the degree of supersaturation is maintained above C_s. Thus, a compact perovskite film is formed. Furthermore, the boiling points of the solvents can be reduced by establishing a low-pressure atmosphere using a vacuum pump in a sealed container and promptly removing the solvents. Hence, the combination of gas flow and reduced pressure can be combined as a better post-treatment to promote the evaporation rate of solvents in the precursor inks and achieve compact perovskite films. This method achieved a PCE of 20.44% (with a device size of 0.1 cm^2).

Moreover, owing to the "soft" nature of perovskites, the secondary grain growth in the extended depth scale can be optimized by surface post-treatment (SISG) [87]. As shown in Fig. 4(b), the minimized surface free energy provided a driving force (ΔF) on the films. In Eq. (2), $\Delta\gamma$ is defined as the anisotropy of surface energy [87]. Similar to the surface free energies of Cs^+ in $CsPbI_2Br$, n-butylammonium (n-BA), octylammonium (OCA), and oleylammonium (OLA) were applied in the SISG process. For the lowest surface energies, films with large grain sizes were achieved with OLA (Fig. 4c). The reduced grain boundary densities were beneficial for photoelectronic behaviour and suppressed the degradation of the devices.

$$\Delta F = F_f - F_i = -\frac{2\Delta\gamma}{h} + \frac{\beta\gamma_{gb}}{\gamma} \quad (2)$$

Furthermore, SCLA has been widely used to control nucleation kinetics with a stable intermediate phase and to reduce the activation energy during nucleation and crystallization processes. As polar aprotic solvents, the commonly used SCLA can coordinate well with PbI_2. However, as shown in Fig. 5(a), rod crystals appeared in the prepared film with pure DMF, leading to poor morphology and coverage. Furthermore, the relatively slow evaporation of the solvents resulted in gaps between the large crystal grains within the films. Therefore, a method for extracting solvents from wet films is required, and the commonly used solvents in the antisolvent process, including 1,2-dichlorobenzene (DCB), butyl acetate (BA), DEE, CB, and EA, are toxic to the environment [88–92]. A solvent-quenching process for volatile solvents has been gradually developed in recent years. As shown in Fig. 5(b), after the antisolvent treatment, a relatively smooth and dense perovskite film was achieved, but pinholes still existed in the films after annealing.

By contrast, after introducing DMSO into precursor inks, the intermediate phase could be formed due to the chemical interaction between DMSO and PbI_2, which could enhance the stability of the coated wet films, resulting in perfect homogeneity compared to samples prepared with pure DMF. Nonetheless, the DMSO molecules in the intermediate wet films cannot rapidly evaporate at ambient temperature, allowing for their extraction during the subsequent annealing process. As shown in Fig. 5(b), the combination of the reduced energy barrier induced by the Lewis bases and the rapid nucleation resulting from the antisolvent process allows for larger grain size and improved contact with substrates. For optimal control of perovskite growth, it is necessary to optimize the balance in the intermediate phase in the films or modify the DMSO concentration in the solvent system. For pure DMSO, less-ordered gain structures were induced by too many intermediate phases in the films, leading to adverse orientation during the annealing process. Therefore, adding a moderate amount of DMSO to a mixed

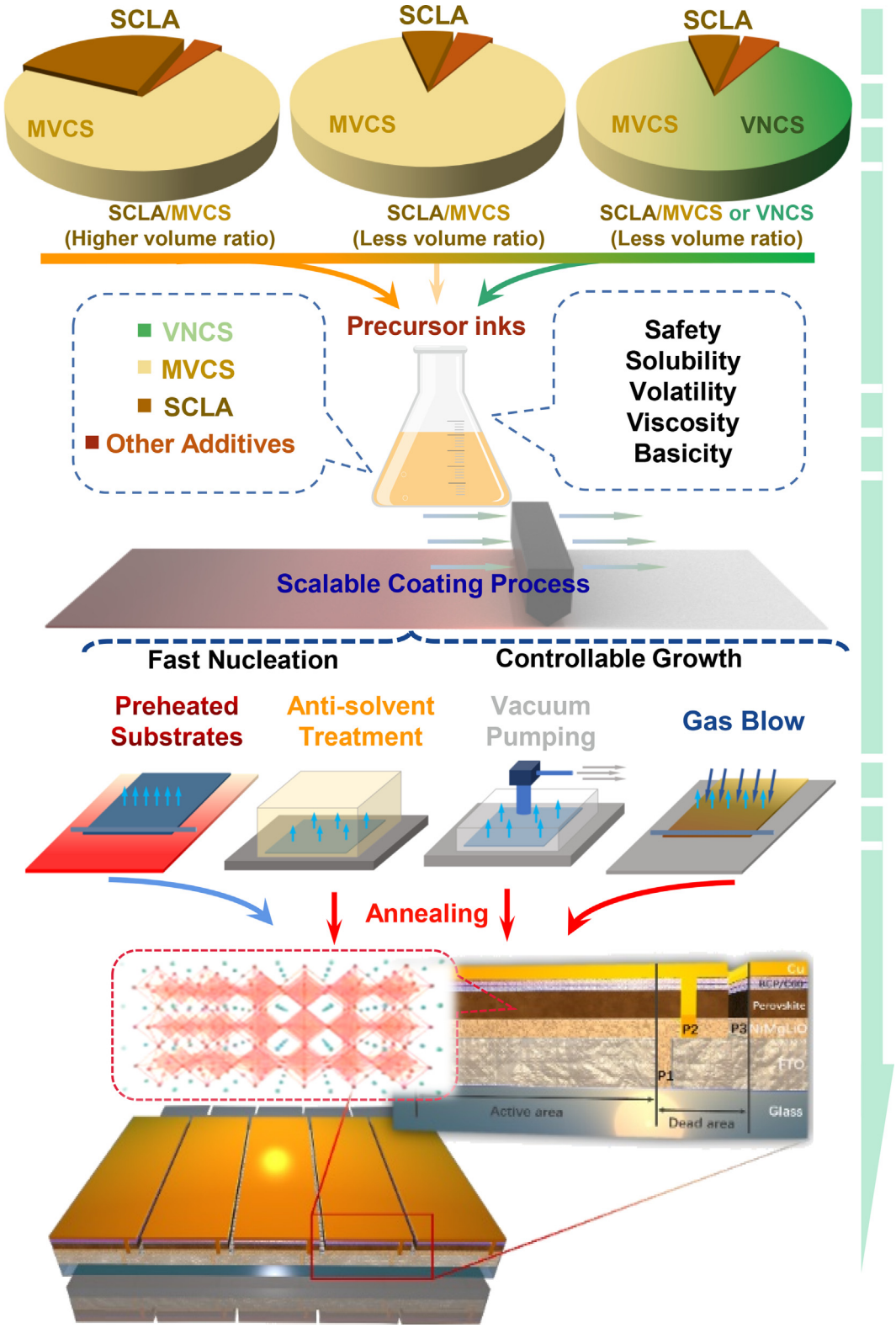

Fig. 3. The progress of solvent mixtures applied for the scalable fabrication of perovskite films. MVCS, moderately volatile, coordinating chemical solvents; SCLA, strongly chelating Lewis bases additives; VNCS, volatile, non-coordinating chemical solvents.

solvent system is beneficial for facilitating the growth of highly orientated perovskite films [93]. Several reports have revealed that the intermediate phase of $MA_2Pb_3X_8(DMSO)_2$ mainly exists in wet-coated films, as shown in Fig. 5(c) [78]. Because the intermediate phase formed in wet films is generally stable at room temperature, it allows for a long processing window during printing and enables the precise preparation of a large-area perovskite film during the synthesis of perovskite crystals. The $MA_2Pb_3X_8(DMSO)_2$ phase underwent annealing and transformed into stoichiometric $MAPbI_3$ with a tetragonal perovskite phase. During

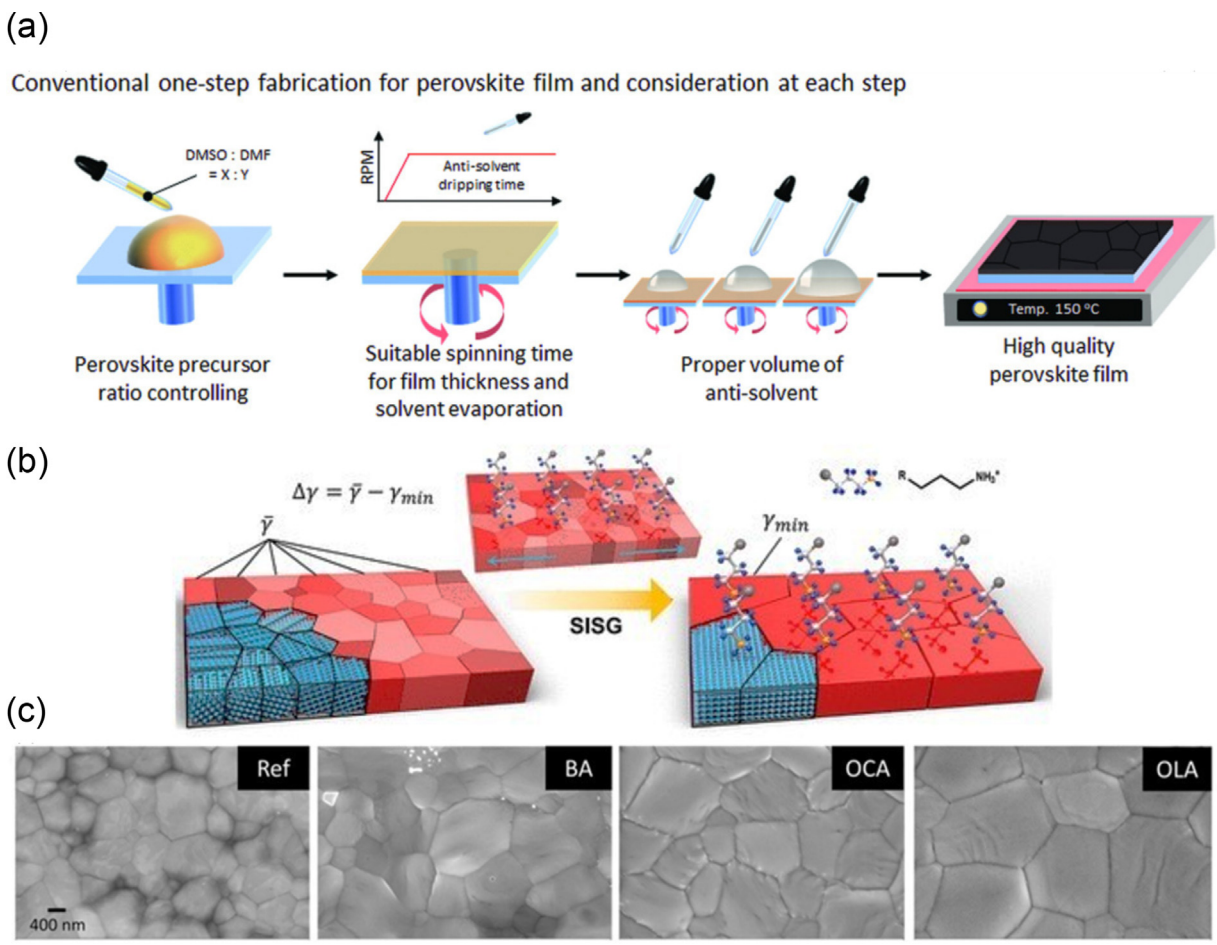

Fig. 4. (a) Preparation of provskite films by spin coating with an antisolvent treatment. Reproduced with permission from Ref. [86]. Copyright 2018, Wiley-VCH. (b) Schematic demonstration of surface-induced secondary grain growth. (c) Surface morphology of the films with different solvents-treatments (IPA, isopropanol; *n*-butylacetate, *n*-BA; octylammonium, OCA; and oleylammonium, OLA). Reproduced with permission from Ref. [87]. Copyright 2019, American Chemical Society.

this process, temperature and time are crucial factors for film quality. A low annealing temperature (<90 ℃) could lead to an incomplete transition of the intermediate phase. This resulted in a higher concentration of the residual intermediate phase and inferior photovoltaic performance of the devices. However, a high annealing temperature could lead to the sublimation of ammonium salt, fast evaporation of DMSO, residual PbI_2, and poorer morphology of the prepared films. Hence, a suitable amount of DMSO and optimized annealing conditions can ensure complete conversion and ideal film morphology.

While solvent evaporation can aid diffusion and bond formation during annealing, intramolecular exchange during intermediate-phase conversion is beneficial for the complex reaction of FA-based perovskites. Yang and co-workers showed that NMP (*N*-methyl-2-pyrrolidone) preferentially interacts with the FA cation (FA^+) over DMSO in FA-based perovskite precursor solutions [94]. As shown in Fig. 5(d), the wet film containing NMP was transparent, whereas the films prepared with DMSO became obscure, indicating a stronger interaction between NMP molecules and the FA cation. By comparing different Lewis bases, Lee and co-workers concluded that the oxygen in NMP and DMI was more sterically accessible to the FA cation. According to studies on acids and bases (HSAB), the MA cation tends to interact with DMSO, whereas the FA cation can form a more stable intermediate phase with NMP. Therefore, a suitable Lewis base can facilitate the stability of the intermediate phase in wet films, which is essential for enhancing their homogeneity over a large area. In addition, solid additives such as NH_4Cl and NH_4I can also be applied to form stable intermediate phases, and NH_4^+ can promote this transformation process without residues remaining in the films. Tong et al. controlled crystallization and achieved compact large-area perovskite films for efficient PSMs (Fig. 5e) [95]. Based on these strategies, the fabricated large-area PSMs achieved a PCE of 14.55% (5 × 5 cm^2) and exhibited a prolonged T_{80} lifetime. In addition, manipulating the growth behaviour of perovskites can also be achieved by modifying the volatility and chemical structure of the solvents (additives) used and the bond formed between the cations and anions in the prepared inks.

The formation pathways for α-$FAPbI_3$ also greatly influence the films [96–98]. In addition to the coordination ability, volatility, and chemical structure of the solvent, Zheng et al. reported that solvent-containing intermediate phases can be classified into two distinct configurations depending on the basicity of the solvent (Gutmann donor number, D_N; Camlet-Taft value, β) [99]. As shown in Fig. 6(a), when β is higher than D_N, the hydrogen bonds between FA^+ and OXR become more robust, and (FA···OXR) PbI_3 intermediates ($D_N < \beta$, SCLA/OXRs) are formed. On the other hand, when β is lower than D_N, PbI_2-OXR is easily formed in the precursor inks. As shown in Fig. 6(b and c), the interaction between FA^+/Pb^{2+} and OXRs played a significant role in the phase transition process. The critical phase transition from intermediate to perovskite involves two processes: the breakage of Pb-O bonds and the formation of Pb-I bonds. Then, the stronger Pb-O bond requires higher energy for breakage, easily leading to the formation of δ-$FAPbI_3$.

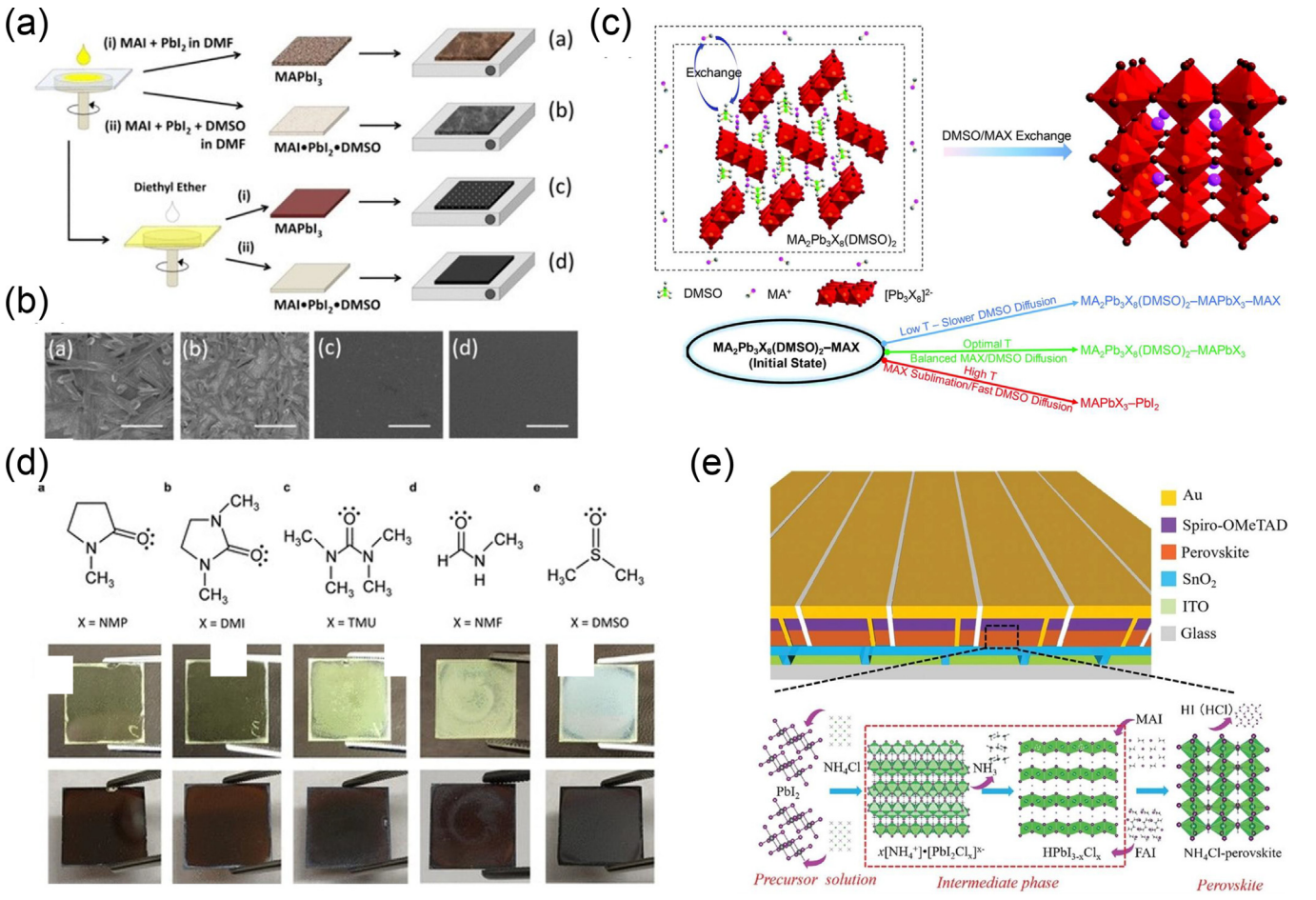

Fig. 5. (a) The preparation process of perovskite films. (b) Top SEM of the perovskite films. Reproduced with permission from Ref. [93]. Copyright 2015, American Chemical Society. (c) Schematic illustration of the intermediate phase and three diffusion ways to final film composition depending on different annealing temperatures; Reproduced with permission from Ref. [78]. Copyright 2016, Royal Society of Chemistry. (d) Optical pictures of films prepared with different Lewis bases. Reproduced with permission from Ref. [94]. Copyright 2018, American Chemical Society. (e) The architecture of the PSMs. Reproduced with permission from Ref. [95]. Copyright 2022, Wiley-VCH.

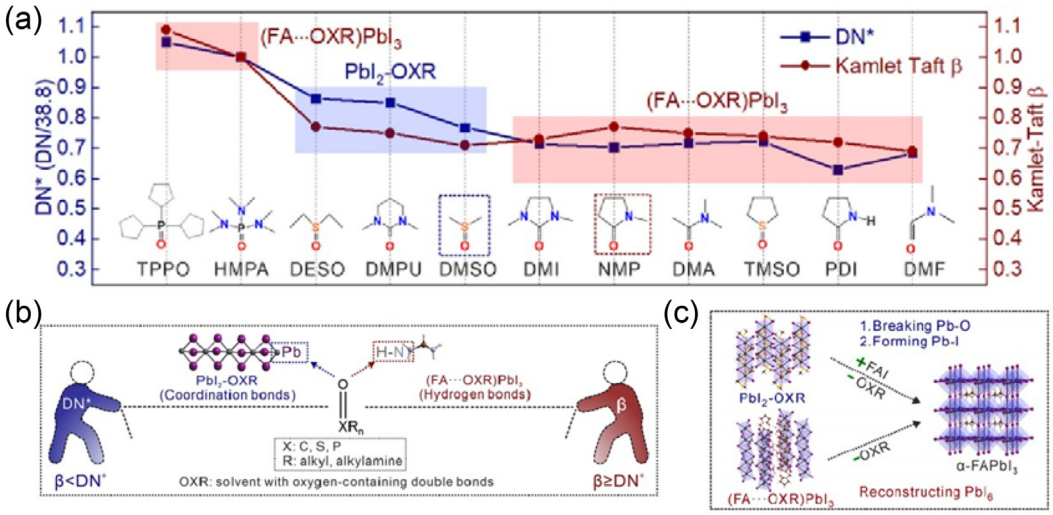

Fig. 6. (a) Summary of solvents and related intermediate structures. (β < DN*, OXR-PbI_2; $\beta \geq$ DN*, (FA···OXR) PbI_3). (b) The interaction ways between Pb^{2+} and SCLA. (c) The structural evolutions of different intermediate phases. Reproduced with permission from Ref. [99]. Copyright 2022, American Chemical Society.

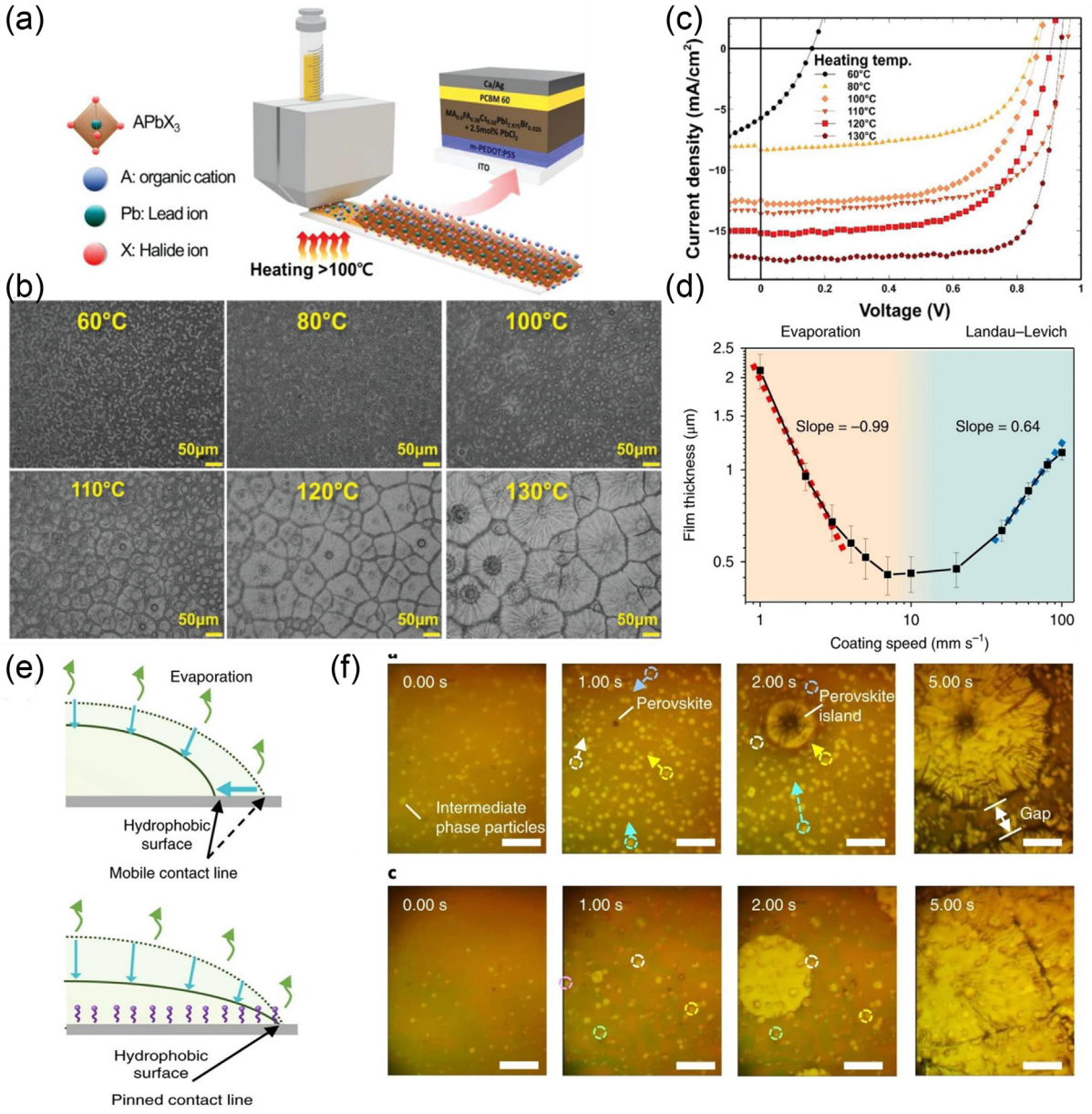

Fig. 7. (a) The illustration of fabricating perovskite films on pre-heated substrates. (b) *J-V* curves of PV devices fabricated on the pre-heated substrates. (c) Optical images of prepared films with different deposition temperatures. Reproduced with permission from Ref. [100]. Copyright 2019, Wiley-VCH. (d) The thickness of prepared films changed with coating speed with precursor inks on a pre-heated substrate (145 °C). (e) The shrinkage of the ink drying process on the different substrates. (f) Observations of in situ microscopy for precursors inks drying dynamics. Reproduced with permission from Ref. [106]. Copyright 2018, Springer Nature.

The Pb-O bonds in (FA···OXR) PbI_3 were relatively lower and helped reduce the energy required for this structural evolution. As a result, they replaced DMSO ($D_N \geq \beta$) with NMP ($D_N < \beta$) in the precursor inks, the formation of α-$FAPbI_3$ was facilitated, and the δ-phase was restricted in FA-based films. Consequently, it is more important than ever to select Lewis bases with a wide range of physicochemical properties to produce high-quality perovskite films.

3. Progress of solvent engineering for PSMs

3.1. Solvents for coating pre-heated substrates

Generally, a higher temperature can promote rapid evaporation of solvents and substrates can be preheated during the coating process. As shown in Fig. 7(a), Kim et al. developed a slot-die coating strategy for preheated substrates to print large-area perovskite films for PSCs [100]. By simply preheating the substrate temperature to 60 °C, the DMF in the mixed solvent system was primarily evaporated. The perovskite crystals, a small amount of DMF, and intermediate phase were the key components in the prepared films. (Fig. 7b). The coating bed temperature was raised from 60 °C to 80 °C, resulting in a homogenous and compact perovskite film owing to the increased evaporation rate of solvents. The corresponding device efficiency improved from 0.31% to 4.26%, as shown in Fig. 7(c). As the solvents in the solutions began to evaporate, larger hexagonal crystals appeared in the films, indicating that the intermediate phase was transformed into the perovskite phase. When the temperature reached 130 °C, the photovoltaic device performance was significantly improved. Based on the optimized preheated temperature, the preparation of perovskite films over a large area by the slot-die coating method was greatly simplified, showing great potential for future industrial applications.

In addition to the pre-heating temperature, the coating speed of precursor inks on preheated substrates is another critical parameter that affects the quality of the target films and corresponding device performance. The optimized thickness of the perovskite film can facilitate the light-harvesting efficiency and carrier transportation. As shown in Fig. 7(d), when the coating speed was relatively low, the precursor inks dried as blade-coating rods moved away from the substrates, and the film thickness was inversely proportional to the speed of motion [101–106]. In the other mode, a thick film was also prepared by accelerating the moving pace of the blade-coating rod, but the films were still wet after the blade-coating rod moved away. Considering the existence of coordinated solvents in wet films and the high surface tension during solvent evaporation, preparing a uniform perovskite film with high quality on the preheated coating bed was difficult. For example, the hole-transport material used in inverted high-efficiency PSCs is PTAA. Although PTAA layers can be readily produced on substrates using a blade-coating technique, perovskite films have limited coverage owing to their poor wettability. To solve this problem, Deng and co-workers prepared perovskite films on a preheated substrate by introducing surfactants into the precursor inks. As the wet films are uniformly spread across the substrates, the rapid evaporation of DMF molecules can be achieved in a short time by pre-heating the substrates, resulting in a fast nucleation process and compact structure in the prepared films. However, during the evaporation of solvents, the complex hydrodynamic process led to inhomogeneous nucleation and growth of crystals over a large area, inducing the "Coffee Ring Effect". The introduction of a surfactant effectively enhanced the viscosity of the precursor inks and their affinity for substrates, as shown in Fig. 7(e). Owing to the complicated fluid flow dynamics in the blade-coating process, large crystal particles grew in the films.

When the particles were heated for an extended time, large gaps developed between them, resulting in films with poor microstructures. (Fig. 7f). Because surfactants lower the surface tension of wet films, they can efficiently improve the homogeneity of films on a wide scale by impeding fluid flow during drying, resulting in a compact film without holes and improved PCEs of the PSMs. In the scalable fabrication of perovskite films, high uniformity is usually required to ensure the photovoltaic performance of each sub-cell, which is essential for the overall performance of the fabricated PSMs.

3.2. Solvents for antisolvent treatment

Aiming at a controllable crystallization process in the scalable fabrication of perovskite films for PSMs, a variety of SCLAs have been introduced to form a stable intermediate phase and improve the crystal quality, as shown in Fig. 8(a). Further research on Lewis base additives is warranted to achieve a more controllable and reproducible fabrication process. Generally, O-donor bases, such as DMSO, are commonly used as polar aprotic solvents to form the intermediate phase PbI_2·DMSO or FAI·PbI_2·DMSO [107–109]. The molecular interactions between PbI_2 and diverse Lewis bases in films can be revealed by Fourier transform infrared spectroscopy (FTIR). As shown in Fig. 8(b), a stretching vibration related to S═O for a bare DMSO appeared at 1045 cm^{-1}. After introducing PbI_2, the shift of the stretching vibration to a lower wavenumber indicated that the PbI_2·DMSO adduct formed.

Upon further dissolving FAI into the inks, hardly any shift in the stretching vibration position indicates the negligible coordination of FAI with DMSO. By introducing thiourea, a kind of solid-state Lewis acid-bases adduct, a gradual shift of the stretching vibration position (S═C) at approximately 1045 cm^{-1} lowered the wavenumber direction, indicating a FAI·PbI_2·thiourea with stronger interaction. After antisolvent treatment, DMF and most of the Lewis bases were extracted from the prepared wet films. If the film originated from an unstable intermediate phase, the film without thiourea gradually became obscure, whereas the film containing thiourea was transparent. Even though DMSO can form an intermediate phase to improve the morphology of $MAPbI_3$ films, the intermediate phase containing thiourea was more suitable for the reproducible synthesis of $FAPbI_3$ films.

Similarly, by employing mixed additives of NMP (liquid) and phenyl sulfoxide (solid, DPSO) into MVCS (DMF) precursor inks, Yang et al. reported that a slot-die-coated wet film (20×14 cm^2) showed a prolonged stable time compared to samples containing only DMF [55]. With a stable molecular structure and stronger interaction energy (Fig. 8c) between DPSO and the solutes in the precursor inks, the wet films can be kept for more time during the fabrication process. Semi-in situ examination at various timeframes depicted in Fig. 8(d) indicates the microstructure development of the coated wet films. This evolution demonstrated the development of a coated wet film microstructure. Adding small amounts of NMP and DPSO to the precursors suppressed unordered growth in wet films. A compact film can be obtained by transitioning the intermediate phase to the stoichiometric perovskite phase during the subsequent annealing process. The crystal grains first appeared in the samples (precursor 1) prepared with pure, indicating the extraction of solvents in the films and weaker interaction with PbI_2. For wet films containing DMF and NMP, crystal grains began to appear in the films after 4 min (precursor 2), indicating that the intermediate phase formed in the films delayed the growth of crystals. With the introduction of DPSO (precursor 3), stronger interactions in the intermediate phase (PbI_2·DPSO) prolonged the time to 8 min, meaning that the dependency of wet films on time was further reduced. Therefore, the complicated production process for perovskite films may be reliably replicated because the intermediate phase with stronger contact makes wet films less dependent on temperature and time. Ultimately, the wet film delivered a dense, uniform perovskite film across a wide area by controlled homogenous crystallization. Based on the optimized parameters, the parallel-interconnected solar module (active area = 20.77 cm^2) achieved a certified PCE of 16.63% (Fig. 8e) and exhibited excellent repeatability (Fig. 8f). The importance of the intermediate phase formed with SCLAs in the process of crystal growth has been reported by many groups, and controllable and uniform crystal growth is essential for upscaling the films. The selection and introduction of Lewis bases will be significant for fabricating PSMs with high efficiency and stability in a reproducible manner in the future [110]. We discuss the solvents design and treatments used in the scalable production of perovskite films for high-efficiency PSMs, except for the solvents system used for the antisolvent.

3.3. Solvents for vacuum flash-assisted methods

By reducing the boiling point, low pressure can facilitate the uniform evaporation of solvents in large-scale wet films and deliver high-quality perovskite films after annealing; this process is called the vacuum-assisted processing method (VASP). Fig. 9(a) shows that the prepared wet film was immediately transferred to the vacuum chamber after the spin-coating process. Most of the solvents were rapidly removed in a low-pressure atmosphere. Then, highly oriented film crystallization can be achieved along with evaporation of the residual solvent during thermal annealing [111]. Recently, the VASP method was developed to prepare perovskite films over a large area for PSMs [112]. The wet films were prepared on substrates using different coating methods, and then a vacuum chamber with low pressure was employed to remove the solvents. Compared with the antisolvent process, which consumes a tremendous amount of toxic solvents, VASP is more environmen-

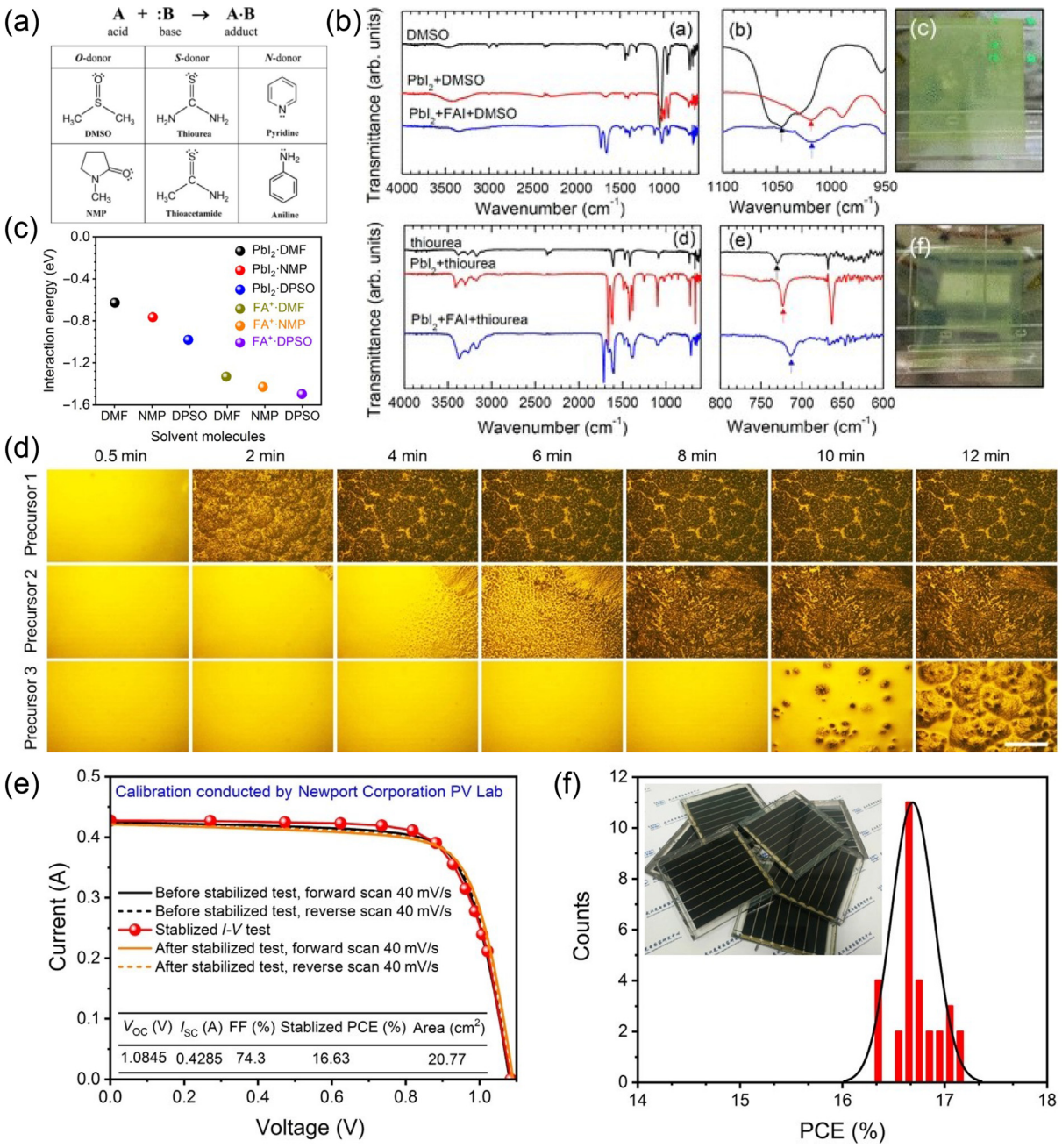

Fig. 8. (a) Reaction between Lewis acid A and base B. (b) The measure on FTIR for SCLA, the photos were the coated films. Reproduced with permission from Ref. [108]. Copyright 2019, American Chemical Society. (c) Interaction energy of additives with the FA^+ and PbI_2. (d) Changes of film morphology over time, observed with an optical microscope (scale bar, 100 um). (e) The *J-V* curves of large-area PSMs with a stabilized efficiency output, and (f) the reproducibility of PSMs. Reproduced with permission from Ref. [55]. Copyright 2021, American Association for the Advancement of Science.

tally friendly and can be used during continuous fabrication. Based on the aforementioned solvent engineering for small-area devices, Li and co-workers coated a GO/QD interlayer to reduce the resistive losses. Consequently, they achieved a certified PCE of 17.85% for PSMs with an aperture area of 17.11 cm^2 (Fig. 9b).

Subsequently, Mai et al. reported that, combined with the related solvents and VASP strategy, a shiny film (4 × 4 cm^2) was achieved after thermal annealing. Similar to conventional SCLA, MACl can also work differently as an additive. As shown in Fig. 9 (c and d), after being treated by vacuum extraction, a small amount of MACl and the intermediate phase containing DMSO resided in the films. As shown in XRD patterns of precursor films prepared by the solution containing DMSO, three diffraction peaks (the blue curve) at approximately 6.63°, 7.25°, and 9.23° can be attributed to the interaction of amine salt and Lewis bases in PbI_2. The absence of diffraction peaks at 12.7° confirmed that the formation of $MA_2Pb_3I_8{\cdot}2DMSO$ intermediate phase predominated in the precursor films, which transform into the tetragonal perovskite phase by low-temperature annealing [113]. After adding the MACl, the diffraction peak at 14.1° became narrower and higher, indicating MACl can help to facilitate the growth of the perovskite phase in prepared films. Accordingly, during the gradual evaporation of MACl, the film possessed a larger grain size than that of the film prepared from the precursor without MACl. Based on the VASP treatment, a small amount of MACl in the precursor inks was introduced to control the morphology and crystallization of the pre-

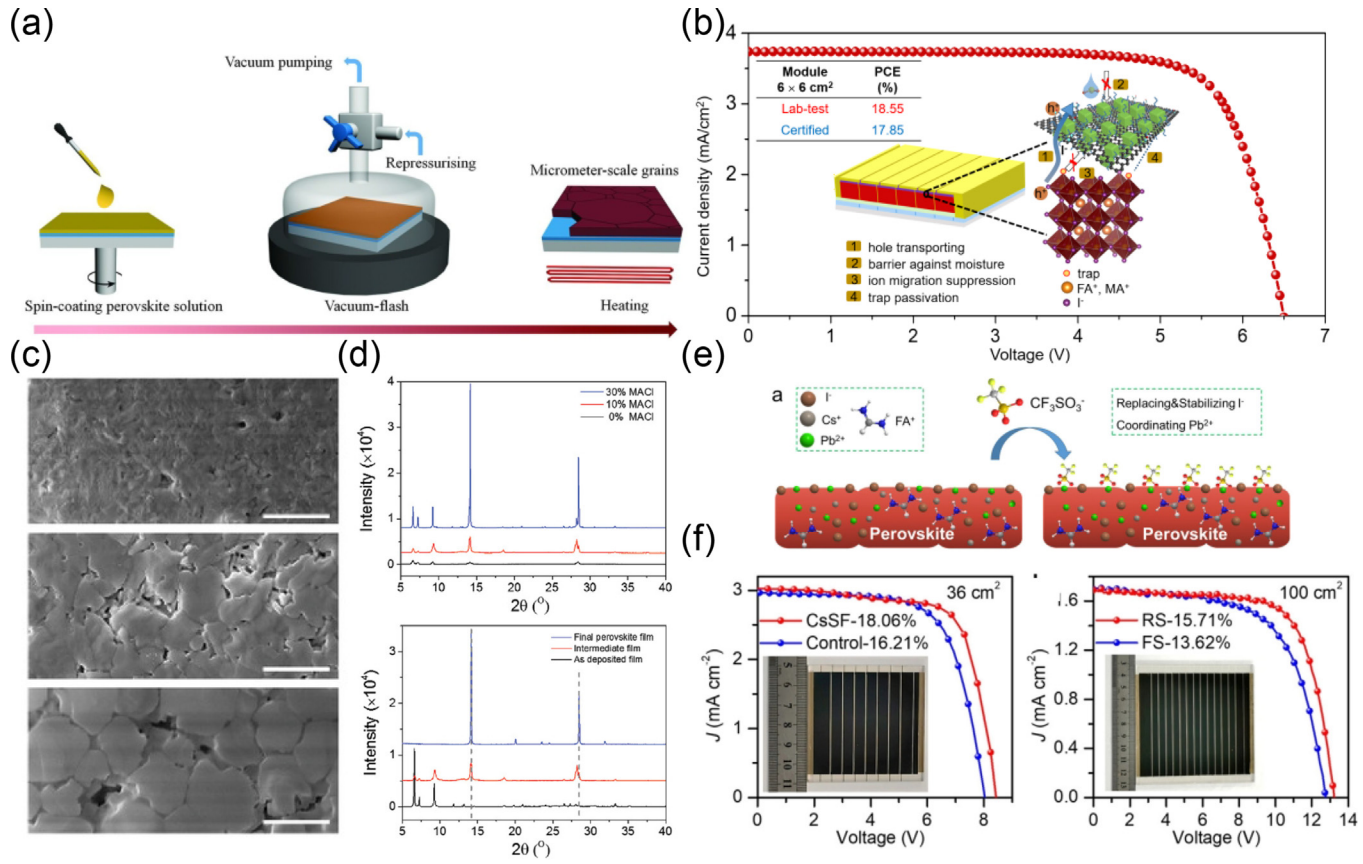

Fig. 9. (a) Scheme illustration of process and crystallization procedures during the formation of films via VASP. Reproduced with permission from Ref. [111]. Copyright 2016, American Association for the Advancement of Science. (b) *J-V* curves and structures of modules. Reproduced with permission from Ref. [112]. Copyright 2022, Royal Society of Chemistry. (c) Surface morphology of intermediate films. (d) The XRD spectra of the coated films assisted with VASP. Reproduced with permission from Ref. [113]. Copyright 2019, Wiley-VCH. (e) The post-treatment with $CsCF_3SO_3$. (f) *J-V* characteristics of PSC modules (36 cm^2 area and 100 cm^2 area). The insets are back-view photos of the PSC modules. Reproduced with permission from Ref. [114]. Copyright 2021, the American Chemical Society.

pared film, and the resultant mini-module (active area = 10.08 c m^2) was fabricated with a PCE of 11.25%. Meanwhile, as shown in Fig. 9(e and f), based on the VASP and related solvents, Chen et al. realized the management of surface iodide by surface chelation on perovskite films with cesium sulfonate (CsF). The prepared PSMs obtained a PCE of 15.7% over a total area of 100 cm^2 [114].

3.4. Solvents for the gas-assisted drying process

3.4.1. Less-volatile solvents for low-speed coating

The time window for the solvent extraction process is also critical, resulting in low fault tolerance in the manufacturing process and limiting the reproducibility of PSMs manufacturing. Although the coating methods combined with antisolvent treatment and VASP can be applied to PSMs, the time window for the non-in situ preparation process severely limits this technique for further mass production. Compared with small-area precursor films prepared in the laboratory, the complete and uniform extraction of solvents from wet films over a large area with an in-situ fabrication process is relatively difficult. Therefore, the in-situ fabrication process is more attractive to achieve a low-cost, stable, and environmentally friendly solar module preparation method for industrial-scale compatible manufacturing. Various solvents and extraction methods have been used to realize an in-situ process for scalable fabrication. Gas-assisted film formation and related solvent design can be substituted for the aforementioned methods.

A blade was used to scrape the perovskite precursor ink to prepare a wet film on the substrate. Uniform horizontal nitrogen was blown from the air knife to accelerate solvent evaporation [115–117]. The pressurized gas flowing through the aerostatic chamber was discharged in a high-strength and uniform laminar flow sheet, which generated a constant linear moving airflow and drove the solidification of the wet films coated on the substrates. In addition, the gas-knife-assisted coating method is suitable for most perovskite-solution systems. Owing to its merits, including the in-situ fabrication process, high reproducibility, and low consumption of chemical reagents, the gas-assisted drying method is promising for up-scaling perovskite films in future industrialised production. To date, many crucial factors closely related to the solvent system design exist for the as-knife-assisted method, such as solution concentration, viscosity, coating speed, slit width, air knife flow pressure, and blowing time [118]. The growth of perovskite crystals can be explained by the classical diffusion-controlled crystal growth model, called the Lamer mechanism, and the Weizmann theory, which is discussed above.

Furthermore, Li et al. proposed associating the supersaturation degree of the precursor inks with the morphology evolution of the perovskite film and connecting it with the performance of related PV devices [119]. As shown in Fig. 10(a), the gas knife-assisted blade coating method is an extensible manufacturing process [118]. Hence, the solvents and related volume ratios in the precursor inks are significant for controlling the growth behaviour of perovskite films over large areas.

However, further studies on the extraction of solvents from wet films and the quality of prepared films are needed and will benefit the development of efficient PSCs and PSMs. Currently, it is still

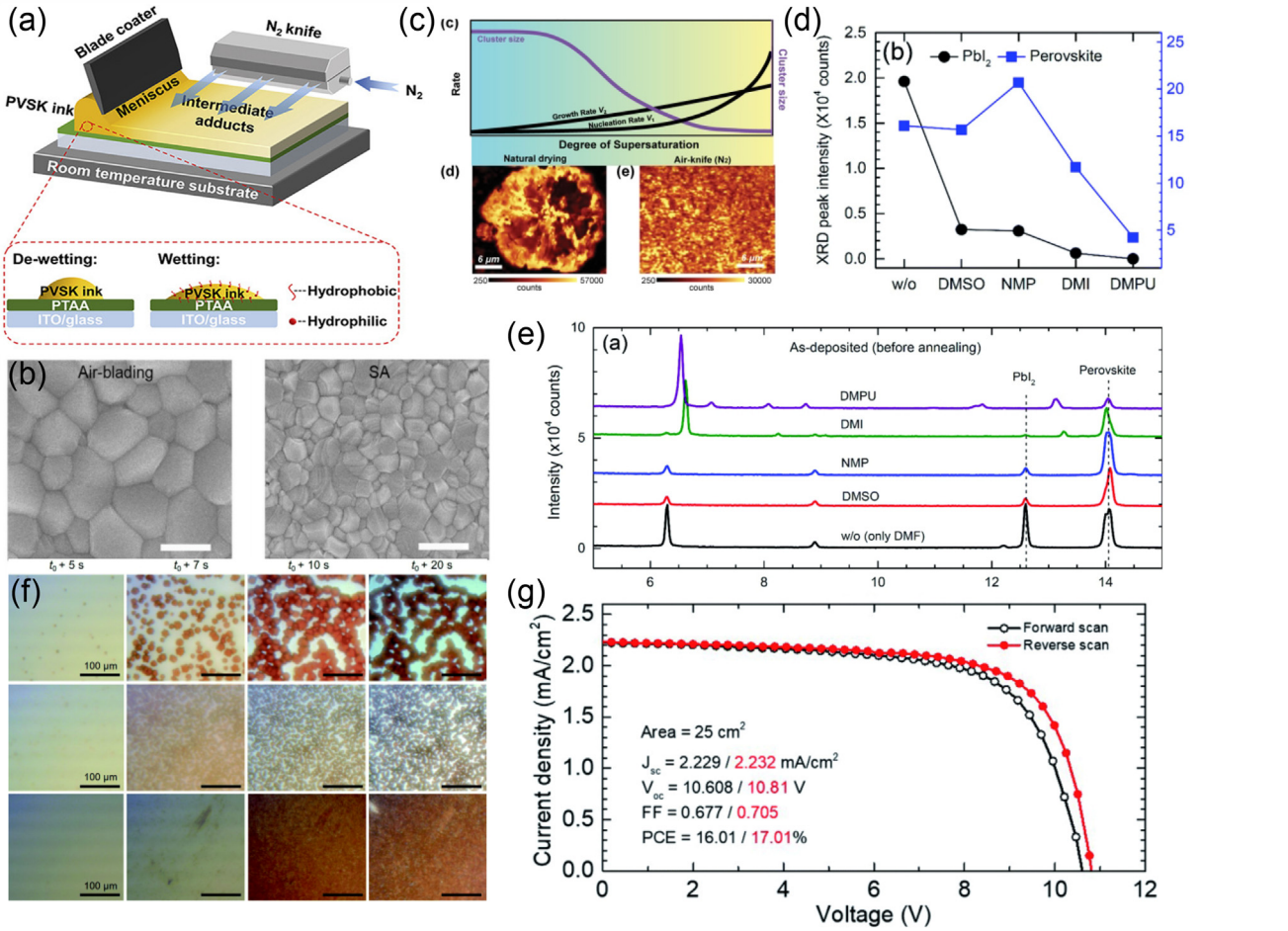

Fig. 10. (a) Schematics of prepared films obtained with a dying-assisted blading process. Reproduced with permission from Ref. [118]. Copyright 2020, Elsevier. (b) Surface morphology of the films with air-blading and SA processes. Reproduced with permission from Ref. [116]. Copyright 2019, Elsevier. (c) Nucleation and growth rates (black line as marked separately) as a function of the supersaturating degree and the spatially resolved PL maps of the films. Reproduced with permission from Ref. [119]. Copyright 2019, Wiley-VCH. (d) The changes of intensities in XRD peaks for PbI_2 and perovskite crystals. (e) XRD curves of films containing different solvents (DMSO, NMP, DMI, and DMPU). Reproduced with permission from Ref. [54]. Copyright 2021, Royal Society of Chemistry. (f) Observations of coated films as a function of air blowing time without and with DMSO/HMPA. (g) The measurement of J-V curves for the prepared PSMs. Reproduced with permission from Ref. [53]. Copyright 2020, Royal Society of Chemistry.

challenging to tailor the solvent coordination in precursor inks to improve the quality of large-area absorption layers. For example, the grain size in an air-bladed film can reach approximately 700 nm, whereas that of the anti-solvent treated (SA-processed) film was only 300 nm (Fig. 10b) [116]. Compared with natural drying, constant flow accelerated the evaporation of the solvents in a linear direction, which ensured the uniformity of the prepared film in the same order. Thus, the application of the gas-knife-assisted blade method requires precursor inks with sufficient volatility at room temperature. Additionally, photoluminescence (PL) mapping of the naturally dried samples revealed a larger perovskite domain with poor substrate coverage, which can be attributed to the impact of the gas flow on the crystallization of the produced films [118]. However, for samples dried by N_2 flow, a uniform PL signal indicated a uniform perovskite film, which highlighted the vital role of the gas blow in this process (Fig. 10c) [120].

Furthermore, after the evaporation of solvents, several additives, such as SCLA, still exist in the films and control the crystal growth behaviour. The Lewis base additives in the inks for the gas-assisted method were beneficial for reducing the time dependency and facilitating crystallization in the subsequent annealing process. However, the instability of the intermediate phase under gas blow caused an unpredictable crystallization process in the precursor films as the SCLA evaporated. Therefore, the Lewis acid-base for the in-situ creation of FA-based perovskites supported with a gas blow requires further investigation. Using blade coating processes, FA-based perovskites may not be compatible with conventional polar aprotic solvents, such as DMSO. Studies on Lewis bases have found that a small amount of these solvents evaporate along with DMF to form holes in the drying process, assisted by a gas-knife flow, leading to poor surface morphology in the films. Park et al. found that diverse Lewis bases with higher donor numbers and boiling points could also be applied in the gas-assisted bar coating process to form stable intermediates [54]. Compared to conventional Lewis bases, the stronger bonding energy between DMPU and Pb^{2+} results in controlled crystal growth. Subsequently, the crystal growth can be analyzed using its XRD pattern, and the characteristic peak of PbI_2 cannot be detected. The related peak intensity of perovskite is much lower than that of other SCLA (Fig. 10d), indicating that DMPU is involved in the formation of intermediates, mainly because DMPU has the highest boiling point and donor number. The relative percentage of the intermediate phase ($F_{\text{intermediatephase}}$) in films can be calculated with A_x representing the peak area at angle ×, as shown in formula (3).

$$F_{\text{intermediatephase}} = \frac{A_{6.54} + A_{7.08}}{A_{6.54} + A_{7.08} + A_{14.04}} \times 100\% \quad (3)$$

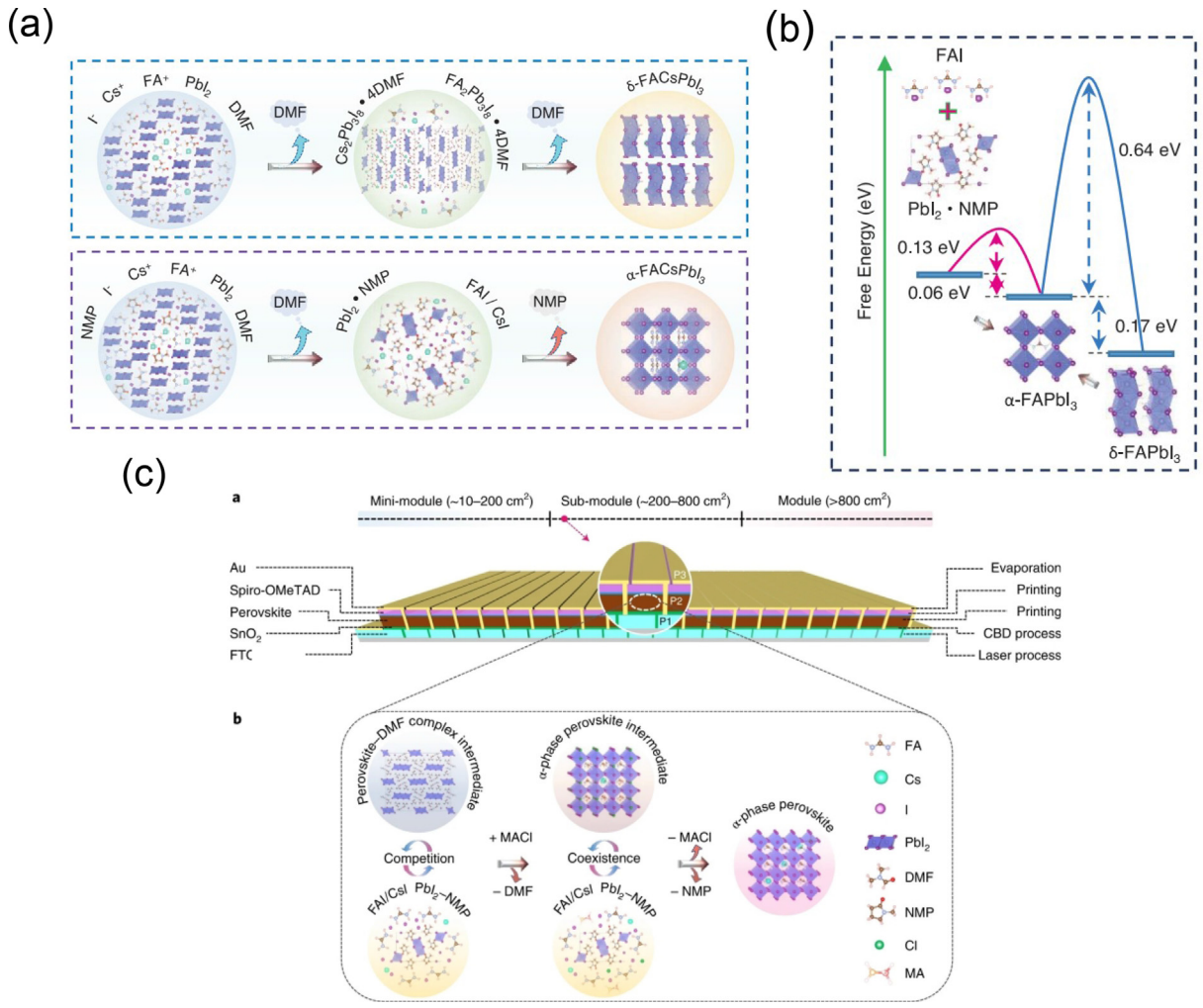

Fig. 11. (a) The illustration of the growth process of perovskite crystals with/without NMP. (b) Calculation of the free energy for the formation of α-$FAPbI_3$ crystals; (a) and (b) Reproduced with permission from Ref. [56]. Copyright 2021, American Association for the Advancement of Science. (c) The phase transition during the removal of MACl. Reproduced with permission from Ref. [125]. Copyright 2022, American Association for the Advancement of Science.

As shown in Fig. 10(e), the peak at 12.6 ° for PbI_2 disappeared after DMPU was introduced into precursor inks. The peak at approximately 14.1° is relatively low, indicating the formation of a stable intermediate phase in films [54,120]. After the subsequent annealing process, the DMPU molecules evaporated from the intermediate phase, and a uniform FA-based perovskite film with fewer defects was obtained. The PCE of the series-interconnection PSMs was 17.94%, indicating better performance than that of the reference samples [54].

These changes can also express the stability of the intermediate phase in the optical microscopic images of the wet films with the air-blowing time. Owing to their physical and chemical properties, Lewis base additives can be used to delay crystal growth with a controllable process, which is necessary to achieve homogeneity at a large scale. They also reported that hexamethylphosphoramide (HMPA) with strong interaction was suitable for forming a stable intermediate phase and successfully prepared an FA-based perovskite film assisted by an N_2-knife (Fig. 10f). Better photovoltaic performance was observed in the perovskite films prepared using HMPA-containing precursor solutions. The perovskite films with better photoelectrical properties exhibited a PCE of 17.01% (Fig. 10g) [53,121]. Despite achieving a homogeneous film over a large area using solvents, tailoring the solvent coordination for perovskite thin films still requires further research.

To study the influence of SCLA additives on the growth process of FAC-based films in depth, Bu et al. analyzed the impact of additives in this process [56]. As shown in Fig. 11(a), following the evaporation of DMF in the precursor inks, the intermediate phases ($Cs_2Pb_3I_8$•4DMF and $FA_2Pb_3I_8$•4DMF) gradually transformed to δ-(FACs) PbI_3. Based on density functional theory (DFT) calculations (Fig. 11b), α-$FAPbI_3$ requires a higher energy for phase transformation. Although even δ-(FACs) PbI_3 can be transformed to the α-phase through a subsequent annealing process, the second phase transformation results in a poor film morphology. In general, the conversation energy can be decreased. After adding NMP to the precursor inks, the intermediate phase PbI_2•NMP restricts the formation of $FA_2Pb_3I_8$•4DMF in precursor inks and is directly transformed to α-(FACs)PbI_3 by reacting with FAI during the subsequent annealing process, avoiding undesired phase transformation and achieving high-quality films [122]. In contrast to NMP, adding MACl to precursor inks can reduce the formation energy needed for the α-phase perovskite crystals and facilitate the transformation of $FA_2Pb_3I_8$•4DMF to the required α-(FACs) PbI_3 (Fig. 11c) [123–125]. Based on the controlled growth process for forming high-quality perovskite crystals over a large area, a PCE of 15.3% for the submodule (aperture area of 205 cm^2) was achieved, as shown in Fig. 11(d). Therefore, introducing appropriate SCLA additives into precursor inks can help realize controllable crystal growth at a large scale.

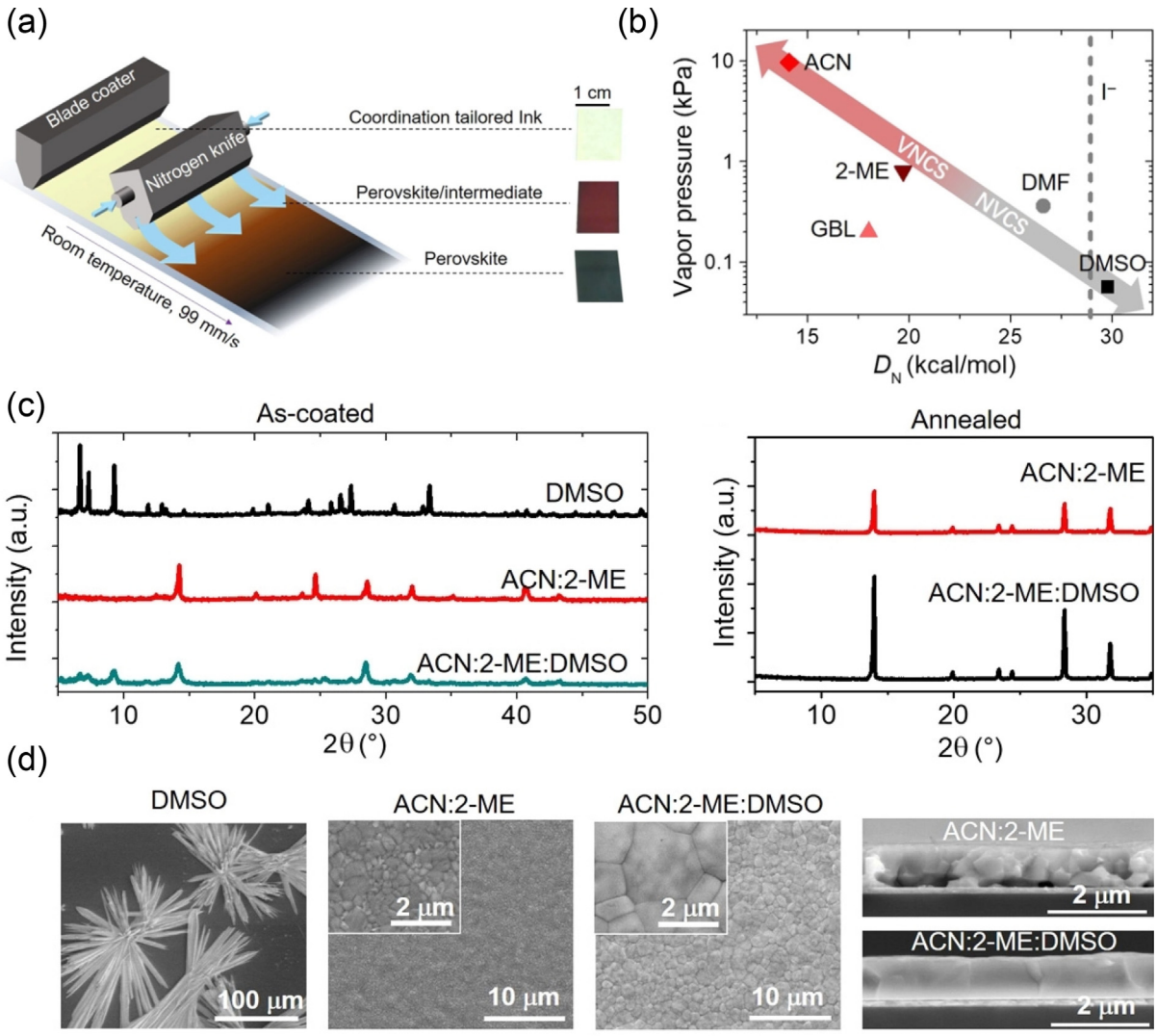

Fig. 12. (a) Schematic illustration for N_2-blow assisted coating of perovskite films at 99 mm/s with tailored ink. (b) Vapor pressure and donor number (D_N) of the solvents. (c) XRD curves of un-annealed films and annealed perovskite films. (d) Surface morphology and cross-sectional images of perovskite films prepared with different solvents. Reproduced with permission from Ref. [126]. Copyright 2019, American Association for the Advancement of Science.

3.4.2. Volatile solvents for high-speed coating

Fast and low-temperature fabrication of perovskite films in a dry atmosphere by introducing VNCS in precursor inks is preferred because it is essential for ensuring the uniformity of coated films over a large area and reducing the time needed for industrial fabrication. Commonly used solvents, such as MVCS and SCLA, cannot satisfy the need for drying in a high-speed coating process. However, pure VNCS, such as 2-ME and ACN, employed in precursor inks can lead to lower crystallinity and poor contact with the substrates, leading to low efficiency and stability of the PSMs. Huang et al. used a new ink design to promote crystallization in films via a N_2-assisted drying process, thereby resolving the contradiction between fast deposition and high crystallinity. The ink comprises VNCS and SCLA at the appropriate volume ratio (Fig. 12a) [126]. Related parameters were analyzed. The D_N of I^- ions in 1, 2-dichloroethane was 28.9 kcal/mol, while the value was much higher than that of 2-ME, CAN, and GBL, indicating that 2-ME and ACN can be used as VNCS (Fig. 12b). The coordination capacity of the solvent refers to the binding strength between the solvents and perovskite precursors, particularly PbI_2. The strong bonding between SCLA and PbI_2 led to the formation of an intermediate phase. To understand the coordination ability of the solvents in detail, the coordination ability of DMSO, DMF, GBL, 2-ME, and ACN to $MAPbI_3$ was investigated in previous research. DMSO and DMF were found to exhibit stronger coordination with PbI_2, whereas GBL, 2-ME, and ACN did not dissolve PbI_2 very well [127,128]. Thus, a combination of two or more solvents at room temperature for the N_2-assisted blade coating can satisfy the need for fast coating and yield large grains (Fig. 12c). The films remained wet following rapid blade coating when DMF, DMSO, or GBL were used as the main solvent. The prepared films were dried at room temperature for a long period of time. In addition to the formation of an inhomogeneous film thickness, the grain size of the perovskite film reached hundreds of nanometres. However, when 2-ME or ACN:2-ME was applied as the only solvent in the blade-coating process, the films rapidly dried and turned black, assisted by N_2 flow, which induced the formation of the perovskite phase, and the grain size generated in the perovskite thin films was less than 100 nm. Although the combination of VNCS with a small amount of SCLA could avoid these shortcomings, the films formed remained dense and uniform. The average grain size of the crystals reached nearly 2 μm, as shown in Fig. 12(d). With these solvent mixtures, a compact perovskite film could be prepared with a fast coating speed of 99 mm/s at room temperature, and the fabricated

PSMs achieved an efficiency of over 16% (with an aperture area of more than 60 cm^2).

In addition, Chen and co-workers reported an improved ink system consisting of 2-ME and ACN for high-speed blade coating and introduced carbohydrazide (CBH) to replace part of the DMSO in precursor inks [129]. In the N_2-assisted blade coating process, all volatile solvents (2-ME and ACN) and most DMSO in the wet films were removed by N_2 flow, resulting in a solid shell on the top of the films. Hindered by the solid top cover, small amounts of DMSO were trapped at the bottom. Residual DMSO evaporated during the subsequent annealing process. The voids in the films were left near the lower interface (Fig. 13a), leading to faster degradation of the perovskite films under light illumination. In addition, introducing a solid additive of CBH reduced the generation of detrimental I_2 during the subsequent aging process in films. The PL emission of the CBH-related sample was more robust and uniform than that of the DMSO-treated sample (Fig. 13b). This contributed to a decrease in voids in the films. The mini-module achieved showed a certified PCE of 19.2% (with an aperture area of 50 cm^2), without significant performance loss after 550 h at 60 °C (Fig. 13c). In contrast, obvious degeneration was observed in samples treated with DMSO. Therefore, in addition to conventional Lewis bases, introducing various solid additives in precursor inks is equally important for the scalable preparation of high-quality perovskite films.

In addition, 1-cyclohexyl-2-pyrrolidone (CHP) can solidly substitute for DMSO to form a stable intermediate phase. Unlike the samples with DMSO, as shown in Fig. 14(a), a black perovskite film can be transformed from a dark yellow film, indicating that the intermediate phase formed with CHP is stable [130]. Hence, the films prepared at a large scale with CHP were more uniform and denser than those prepared with DMSO (Fig. 14b). Meanwhile, inorganic solid additive ammonium chloride (NH_4Cl) can also be used to control the growth of crystals in films on flexible substrates. Dai et al. employed additive engineering to prepare high-quality perovskite films on flexible Corning Willow glass. NH_4Cl can prevent nucleation in perovskite films, thus avoiding the formation of cavities between the perovskite films and the glass interface. The $MAPbI_3$ solutions in 2-ME (Fig. 14c) were entirely dissolved, and N_2 gas was used to remove part of the solvent to form a supersaturated solution with black perovskite clusters. Then, after adding NH_4Cl powder to the supersaturated solution while stirring at room temperature, the precursor ink became clear again, and the clusters completely dissolved within 1 min, indicating that NH_4Cl enhanced the solubility and dissolved the precipitated perovskite clusters [131–133]. Consequently, after the residual solvents escape from the valley under the top layer, the films tend to grow from the top to bottom. By inhibiting nucleation for slow curing, most precursor inks, especially those in the valley, have sufficient time to form good contact with flexible substrates. Thus, the efficiencies of the devices prepared by adding ammonium chloride were 15.0% for small-area PSCs and 15.8% for PSMs with an aperture area of 42.9 cm^2. This work demonstrates the critical role played by the NH_4Cl additive for films on flexible substrates (Fig. 14d).

In a volatile chemical ink system, reducing the use of SCLA can minimize the time required for the subsequent annealing process,

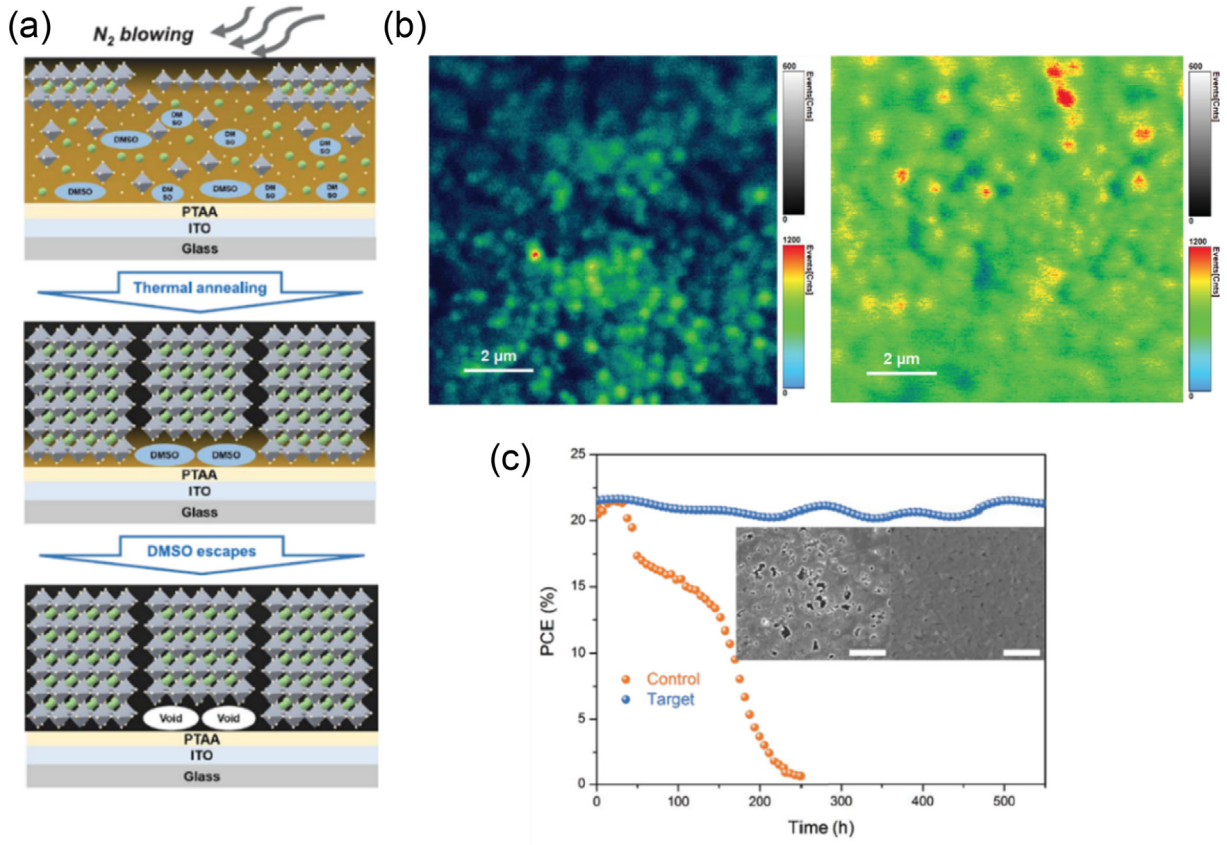

Fig. 13. (a) Illustration shows the formation of voids at the interfaces (perovskite/substrate). (b) PL mappings of the control (left) and target perovskite films(right) on glass excited with a 485 nm laser. (c) Operational stability tests of the encapsulated control and target PSCs under 1-sun equivalent illumination in air. The inset was the top-view SEM images of the peeled-off perovskite-substrate interface of the light-soaked control (left) and target(right). Scale bars were 1 mm (Inset). Reproduced with permission from Ref. [129]. Copyright 2021, American Association for the Advancement of Science.

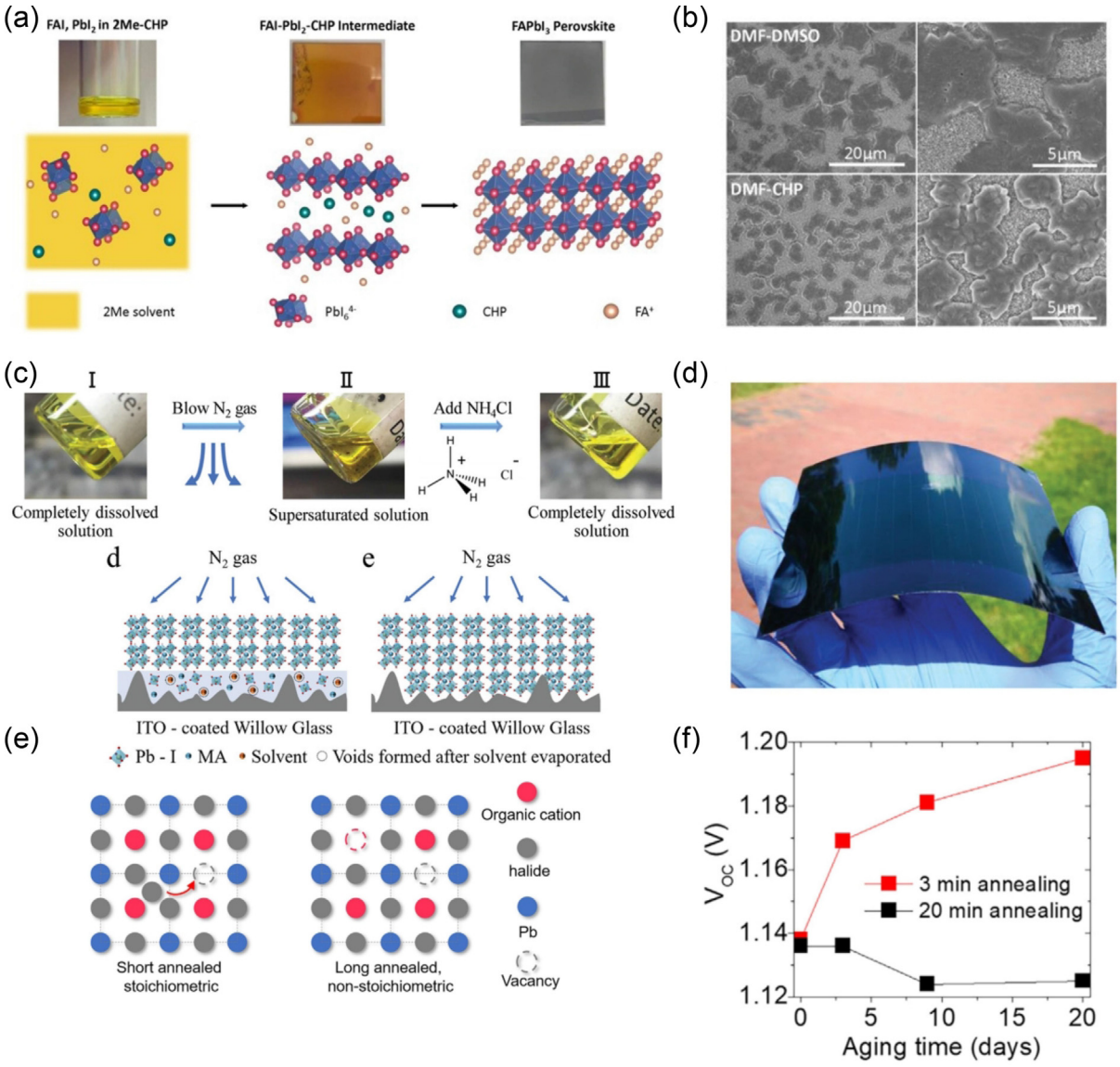

Fig. 14. (a) The illustration of film formation in mixed solution(2ME-CHP). (b) The surface morphology of the films. Reproduced with permission from Ref. [130]. Copyright 2021, Elsevier. (c) The schematic illustration of perovskite films on ITO-coated Willow Glass. (d) Optical photograph of the flexible perovskite module. Reproduced with permission from Ref. [133]. Copyright 2020, Wiley-VCH. (e) The structure transition of perovskite materials annealed for 3- and 20-min. (f) Variation of (open circuit voltage) V_{oc} as a function of illumination intensity for 0, 3, 9, and 20 days. Reproduced with permission from Ref. [134]. Copyright 2020, Elsevier.

which is cost-effective for manufacturing and transportation. Deng et al. demonstrated that a reduced self-doping mechanism with a short-time annealing process could enhance the photovoltaic performance of the resultant PSMs. The self-doping level of perovskite materials is suppressed by reducing the annealing and aging times at room temperature (Fig. 14e) [134]. Reduced self-doping results in less charge recombination and improves the photovoltage output. Scalable fabrication of perovskite thin films can be achieved with a short annealing time (3 min), as shown in Fig. 14(f). At a 1/4 sun intensity (25 mW/cm^2), the aperture efficiency of the mini-module reached 18.7%. Shortening the thermal annealing time can maintain the stoichiometric composition of the perovskite crystals and restrict the spontaneous de-doping of the as-fabricated films. A similar phenomenon can also be observed in FACs film-based PSMs, indicating that the short-time annealing process has universal applicability for preparing efficient PSMs. Furthermore, perovskite films annealed for a shorter time are more stable for storage, which can further enhance the commercial competitiveness of this emerging PV technology.

3.5. Solvents engineering and performance of PSMs

Developing a stable, low-cost, and environment-friendly solvent system for upscaling perovskite films is of great significance for improving the photovoltaic performance of PSMs. Moderating solvent mixtures (solvent engineering) plays a decisive role in the coating process for the quality of films over large areas. With respect to the commonly used solvent system, a confirmed volume ratio of highly volatile solvents is needed to promote the concentration of wet films to reach supersaturation within a short time. Then, a smaller amount (compared to the volume ratio of highly volatile solvents) of Lewis base additives is needed to form a stable intermediate phase to prolong the time window and promote further growth of perovskite crystals [135–141]. In addition, the cost and toxicity of solvents should also be crucial factors for carefully considering the solvent system design rules for films. According to relevant reports in recent years, commonly used solvents and Lewis base additives are used for the photovoltaic parameters of the corresponding modules (Table 3). DMF has played an indis-

pensable role in the fabrication process and is a solvent with excellent solubility for most perovskite materials, moderate volatility, and coordination ability. Deng and co-workers used pure DMF as the solvent during the coating process on preheated substrates. With a small amount of L-a-phosphatidylcholine, the homogeneity of the growth behaviour at a large scale is improved [106].

For a controllable growth process of perovskite crystals, a high volume ratio of liquid Lewis bases (volume ratio of approximately 25%) is generally introduced into DMF. During the antisolvent treatment, DMF and most of the Lewis base additives in the precursor films were removed, yielding the preliminary perovskite films. The intermediate phase formed with residual Lewis base addition not only prolongs the processing window of the as-coated wet films but also promotes the further growth of perovskite crystals in the subsequent annealing process. Using mixed solvents of DMF and DMSO (volume ratio = 4:1), Huang et al. prepared films (10×10 cm^2) with an antisolvent bath and achieved a module efficiency of 13.85% [48]. In addition, based on a similar solvent system (DMF/DMSO, volume ratio = 4/1), Nazeeruddin et al. achieved a recorded PCE of 19.0% on V1366 layers (the active area of PSMs was 30.24 cm^2) [66]. By introducing solvent mixtures of DMF, NMP, and DPSO, Yang et al. prepared a high-quality $FA_{0.83}Cs_{0.17}PbI_{2.83}Br_{0.17}$ film over a large area with a controlled fabrication process. They achieved parallel-interconnected modules with a certified PCE of 16.63% [55]. As reported by Zhu et al., heptadecafluorooctanesulfonic acid tetraethylammonium salt (HFSTT) is also a potential substitute additive for fabricating uniform films over large areas, and the PSMs exhibited a PCE of 21.05% (with an active area of 25.98 cm^2) [142]. Although antisolvent treatment has matured as a technology for scalable manufacturing of perovskite films, the use of a large variety of solvents in this process not only increases the price of PSMs, but also increases environmental and security concerns. [143–147].

To avoid wasting solvents in the antisolvent bath, the solvents designed for VASP also need further modulation; this modulation is mainly achieved by reducing the volume ratio of Lewis base additives in precursor inks. Assisted by a low-pressure atmosphere, the fast evaporation of DMF contributes to a rapid nucleation in precursor films, and the Lewis base additives with a high boiling point only evaporate during the subsequent annealing process. The intermediate phase from the interaction between the Lewis base and solutes can avoid the negative influence of excessive growth on the surface morphology of the prepared films and promote crystal growth by reducing the formation energy. Using the solvent mixtures designed for VASP, Li, and co-workers employed the cross-linked 1D Pb_3I_6-DPPO (1D-PbI_2) complex with ethane-1,2-diylbis (diphenylphosphine oxide) (DPPO) to passivate defects caused in the film formation process and achieved a certified PCE of 17.8% for PSMs with an active area of 17.11 cm^2 [65]. In addition, Mai and co-workers have applied MACl to further improve the crystallization of films in the intermediate phase, achieving a resultant PCE of 18.06% for prepared PSMs with an active area of 18.00 cm^2 [113]. Then, they introduced a small amount of 4-guanidinobutanoic acid additives to form 2D and 3D perovskite heterostructures and achieved a PCE of 14.48% for PSMs on flexible substrates with an active area of 10.64 cm^2 [148]. In addition, based on mixed solvents (DMF/NMP), Chen and co-workers restrained the movement of perovskite colloidal particles in wet films using the sticky functional groups in Bio-IL; the fabricated PSMs (the active area was 14.63 cm^2) achieved a PCE of 16.87% [149].

Other Lewis bases with high donor numbers, such as HMPA and DMPU, can also substitute for traditional DMSO in the gas-assisted film formation process. Furthermore, owing to the strong polarity and high boiling point of DMPU, the stable intermediate phase structure further promotes the uniformity of the prepared films over a large area. In based solvents systems (DMF/DMPU), Park and co-workers have reported a PCE of 17.94% for PSMs with an active area of 19.96 cm^2 [53]. In addition, by adding alkali salts ($CsPbBr_3$, $KPb2Br_5$), Mathews and co-workers have slot-die coated uniform FACs films (100 cm^2) with high crystallinity assisted by N_2 blow post-treatment and achieved a PCE of 16.22% for the fabricated mini-module with an active area of 57.5 cm^2 [57]. However, although DMF can evaporate at room temperature, the slow evaporation rate restricts the coating speed, which cannot meet the gas-assisted high-speed coating process demand. Therefore, Deng et al. replaced DMF with ACN and 2-ME in precursor inks and rapidly dried the wet films using N_2 flow, calling for a high-speed coating technique, during which a rapid nucleation and growth process for perovskite crystals has been achieved. In addition, combined with a small amount of intermediate phase formed by Lewis bases such as DMSO and NH_4Cl, films with compact structures and large grain sizes have been achieved with controllable growth behaviour of perovskite crystals in the subsequent annealing process [129]. Then, as reported by Chen and co-workers, the solid Lewis base additive CBH was an excellent choice for partially replacing the liquid DMSO to avoid the appearance of voids near the interface during the annealing process and to achieve PSMs with better stability under illumination. In addition, compared to the use of SCLA in antisolvents-related solvent systems, the use of SCLA in precursor inks for air blow-assisted in situ preparation was drastically reduced. In addition, reducing the volume ratio of SCLA in the solvent system shortens the time required for the subsequent annealing process, thereby decreasing the cost of fabrication.

Although the high volatility of 2-ME and ACN in precursor inks is beneficial for realizing a rapid nucleation process, their poor solubility in inorganic perovskite materials has limited their widespread application in various perovskite materials. In precursor inks containing MVCS and several other SCLAs with higher polarity, most inorganic perovskite materials can be fully dissolved [150,151]. Hence, to coat perovskite films with various compositions over a large area, the solvent mixtures must be further regulated according to the physical and chemical properties of the solvents to develop a solvent system with better material compatibility and process control. The high boiling point, suitable chemical structure, and strong interaction with lead halides can keep the intermediate phase stable at room temperature [152–155]. However, according to the basicity of the solvents and their interactions with solutes, the selection and ratio of Lewis bases (liquid or solid) introduced into the inks need to be more precise. Excessive or fewer Lewis base additives may lead to the appearance of holes in perovskite films during the annealing process, resulting in poor photovoltaic performance and stability of PSMs. Considering its critical role in the fabrication process, solvent selection and usage are essential for improving the quality, uniformity, and reproducibility of perovskite films over a large area.

4. Alternative nonhazardous solvents in solvent systems

In the development of industrial manufacturing of PSMs, the large consumption of solvents such as DMF, NMP, DMSO, and DMAC used in the scalable fabrication of perovskite films has a significant impact on the natural environment, especially in terms of health and safety [156–163]. The criterion for defining safe solvents is non-toxicity to humans after exposure during manufacturing. Vidal et al. studied the risks of polar aprotic solvents used in conventional ink systems, as shown in Fig. 15(a) [164]. The Human health characterisation factors expressed in disability-adjusted life years (DALY) per kilogram of solvents can act as the measurement of the danger induced by the solvents. It is alarming that the most commonly used solvents in precursor ink systems and DMF have

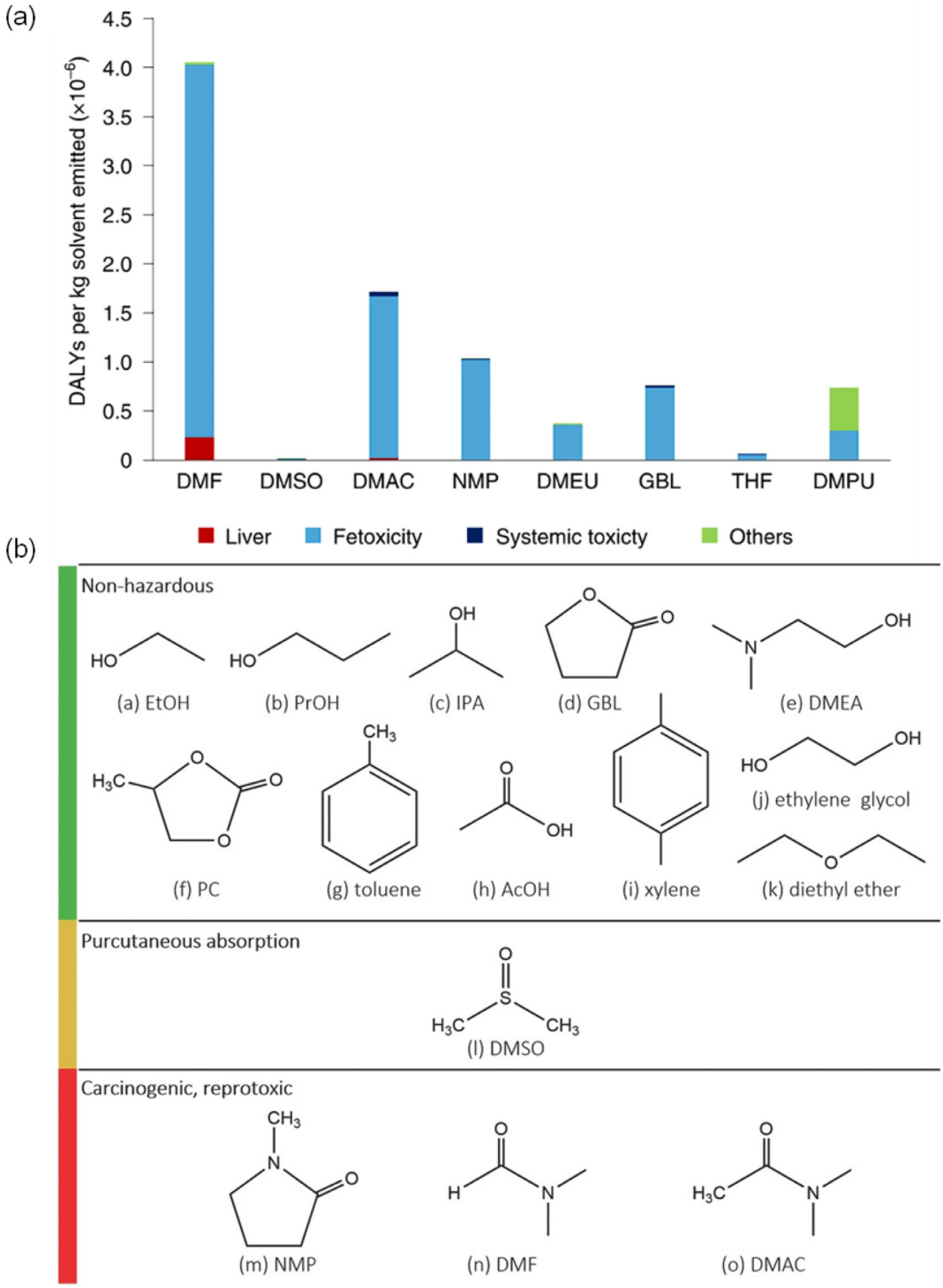

Fig. 15. (a) Influence of commonly used solvents in precursor ink system on health. (Mainly focusing on the liver, fetotoxicity, systemic toxicity, and other aspects). The DALY represents disability-adjusted life year per kg of solvents; Reproduced with permission from Ref. [164]. Copyright 2021, Springer Nature. (b) The diagram on the safety of the solvents in precursor dissolution is divided into nonhazardous, absorbable through the skin, and carcinogenic and repro-toxic solvents. Reproduced with permission from Ref. [165]. Copyright 2016, Wiley-VCH.

the highest DALY values. In addition to its destructive impact on the liver, DMF has also been identified as a harmful substance to fetal growth. Additionally, dimethylacetamide (DMAC), NMP, and DMPU are toxic to humans. As reported by Gardner et al., the risks associated with various solvents are shown in Fig. 15(b) [165]. DMF, NMP, and DMAC are toxic and can easily cause cancer, and DMSO can be absorbed through the skin. Ethyl alcohol (EtOH), IPA, GBL, ethylene glycol, diethyl ether, toluene, and acetic acid (AcOH) are non-hazardous solvents.

However, as reported by the related medical articles, the 2-ME and Ethyl ether have been recognized as safe solvents for many medical treatments and measurements. Furthermore, compared to the commonly used MVCS and SLCA, most VNCS are relatively safe for humans [166–169]. Hence, considering the toxicity, the

selection of solvents in precursor inks must decrease the use of MVCS and SLCA and promote the wide use of VNCS, which is consistent with the aforementioned suggestion regarding improving solvent engineering.

5. Challenges and suggestions for further development

Compared to small-area perovskite films, up-scaling high-quality films requires a moderately prolonged processing window for controlled crystal growth. Despite tremendous efforts in solvent engineering devoted to the scalable coating of perovskite films for efficient PSMs, an appropriate green solvent system for industrial production is still desired. By adjusting the concentration, volatility, viscosity, interactions between the solvents and solutes, and coating temperature of the precursor inks, the crystallization dynamics of the perovskite films can be precisely manipulated. Based on the solvents system, the corresponding post-treatments, such as pre-heating the coated substrates, vacuum flash or pump, gas blowing, and antisolvent baths, can accelerate the supersaturation of precursor inks and play an essential role in realizing rapid nucleation and controllable growth processes over a large area.

In conclusion, various VNCS, MVCS, and SCLA are necessary solvents in the solvent system to move perovskite precursor ink towards scalable coating technologies and play a prominent role in related design rules. Utilization and associated physicochemical properties are listed in Table 4 and Table 5. Commonly used MVCS, such as DMF, can dissolve most inorganic perovskite materials at room temperature, but its slow evaporation leads to uncontrollable nucleation and random crystal growth, resulting in heterogeneous perovskite films. Furthermore, solvents with strong coordination ability and low vapour pressures have been introduced, such as the Lewis bases of NMP, DMSO, DMPU, and DMI; these solvents form stable intermediate phases in wet films. However, stronger interactions between the solvents and solutes, make the complete extraction of the solvent molecules in the fabricated wet films more difficult; in addition, too much SCLA adversely affects the crystal growth during the subsequent annealing process. Although a suitable antisolvent bath strategy has been developed, the mass use of antisolvent may increase the safety risks and manufacturing costs.

To accelerate the industrialization of PSMs, a fast and continuous fabrication process for perovskite films over a large area should be reproducible, inexpensive, and environmentally friendly. Furthermore, owing to its low boiling point, VNCS can be easily extracted by a simple post-treatment. However, for volatile solvent systems such as ACN/2-ME mixed solvents, the poor solubility of inorganic halide salts is still a large challenge and restricts their widespread application. Therefore, considering the different physicochemical properties of VNCS, MVCS, and SCLA, suggestions for improving solvent engineering are listed below and schematically depicted in Fig. 16.

(1) The evaporation, solubility, and toxicity of the primary solvents in the precursor ink should be balanced, and MVCS must be partly replaced by VNCS.
(2) A small amount of SCLA can realize a controllable growth process for high-quality perovskite crystals.
(3) Apart from avoiding the waste of solvents, in-situ fabrication processes, such as N_2-assisted blade coating and related solvent mixtures, can be used to enhance the reproducibility of the scalable fabrication process.

In addition to avoiding the waste of solvents by the conventional anti-solvent bath, mixed solvents containing both MVCS and VNCS can satisfy the need to completely dissolve most types of perovskite solutes and rapidly evaporate solvents by regulating the ratio. In addition, a small amount of suitable Lewis bases or solid additives is essential to grow perovskite crystals and extend the time window, resulting in a controllable crystal growth process. Simultaneously, this improved solvent system can also be suitable for a high-speed in situ fabrication process, ensuring high reproducibility and low cost of this technique for future continu-

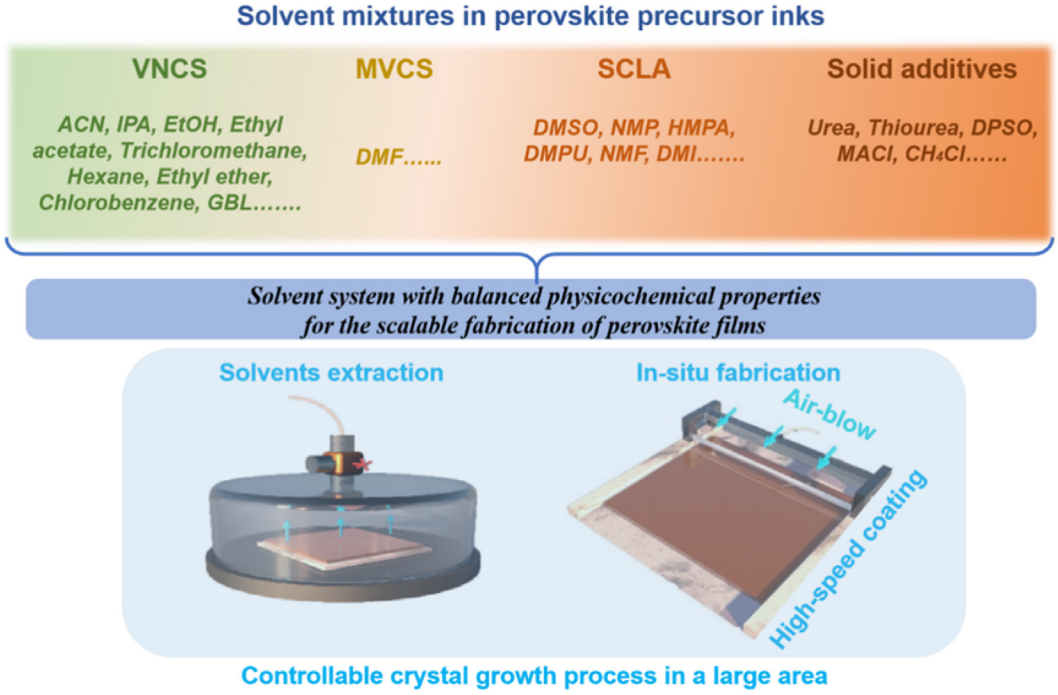

Fig. 16. Schematic illustration of a novel solvent system strategy toward the scalable fabrication of perovskite films.

ous fabrication. Therefore, except for the introduction of more suitable solvents, a novel solvent system design strategy for scalable fabrication of perovskite films should be preferred to promote the future industrialization of high-efficiency PSMs.

Declaration of competing interest

The authors declare that they have no known competing financial interests or personal relationships that could have appeared to influence the work reported in this paper.

Acknowledgments

This work was financially supported by the National Key Research and Development Project funding from the Ministry of Science and Technology of China (2021YFB3800104), the National Natural Science Foundation of China (51822203, 52002140, U20A20252, 51861145404, 62105293, 62205187), the Young Elite Scientists Sponsorship Program by CAST, the Self-determined and Innovative Research Funds of HUST (2020KFYXJJS008), the Natural Science Foundation of Hubei Province (ZRJQ2022000408), the Shenzhen Science and Technology Innovation Committee (JCYJ20180507182257563), Fundamental Research Program of Shanxi Province (202103021223032), and the Innovation Project of Optics Valley Laboratory of China (OVL2021BG008).

Appendix A. Supplementary material

Supplementary data to this article can be found online at https://doi.org/10.1016/j.jechem.2023.02.017.

References

[1] H. Zheng, M. Song, Z. Shen, Energy 237 (2021).
[2] M.A. Green, A. Ho-Baillie, H.J. Snaith, Nat. Photonics 8 (2014) 506–514.
[3] M.C. Kim, S.Y. Ham, D. Cheng, T.A. Wynn, H.S. Jung, Y.S. Meng, Adv. Energy Mater. 11 (2021) 2001753.
[4] Y. Rong, Y. Hu, A. Mei, H. Tan, M.I. Saidaminov, S.I. Seok, M.D. McGehee, E.H. Sargent, H. Han, Science 361 (2018) eaat8235.
[5] Z. Zhu, K. Mao, J. Xu, J. Energy Chem. 58 (2021) 219–232.
[6] J. Wang, J. Liu, Z. Du, Z. Li, J. Energy Chem. 54 (2021) 770–785.
[7] C. Zhou, A.B. Tarasov, E.A. Goodilin, P. Chen, H. Wang, Q. Chen, J. Energy Chem. 65 (2022) 219–235.
[8] X. Zhou, J. Jankowska, H. Dong, O.V. Prezhdo, J. Energy Chem. 27 (2018) 637–649.
[9] A. Kojima, K. Teshima, Y. Shirai, T. Miyasaka, J. Am. Chem. Soc. 131 (2009) 6050–6051.
[10] M.A. Green, A. Ho-Baillie, ACS Energy Lett. 2 (2017) 822–830.
[11] Y. Ma, Q. Zhao, J. Energy Chem. 64 (2022) 538–560.
[12] W. Zi, Z. Jin, S. Liu, B. Xu, J. Energy Chem. 27 (2018) 971–989.
[13] M.A. Green, E.D. Dunlop, G. Sierfer, M. Yoshita, N. Kopidakis, K. Bothe, X.J. Hao, Prog. Photovoltaics 31 (2023) 3–16.
[14] Y. Deng, G. Ren, D. Han, W. Han, Z. Li, C. Liu, W. Guo, J. Energy Chem. 73 (2022) 615–638.
[15] L. Qiu, S. He, L.K. Ono, S. Liu, Y. Qi, ACS Energy Lett. 4 (2019) 2147–2167.
[16] H. Li, J. Zhou, L. Tan, M. Li, C. Jiang, S. Wang, X. Zhao, Y. Liu, Y. Zhang, Y. Ye, Sci. Adv. 8 (2022) eabo7422.
[17] M. Du, S. Zhao, L. Duan, Y. Cao, H. Wang, Y. Sun, L. Wang, X. Zhu, J. Feng, L. Liu, Joule 6 (2022) 1931–1943.
[18] Y. Yang, Z. Xue, L. Chen, C.F.J. Lau, Z. Wang, J. Energy Chem. 59 (2021) 626–641.
[19] Z. Li, T.R. Klein, D.H. Kim, M. Yang, J.J. Berry, M.F. Van Hest, K. Zhu, Nat. Rev. Mater. 3 (2018) 1–20.
[20] Y. Rong, Y. Ming, W. Ji, D. Li, A. Mei, Y. Hu, H. Han, J. Phys. Chem. Lett. 9 (2018) 2707–2713.
[21] M. Yang, D.H. Kim, T.R. Klein, Z. Li, M.O. Reese, B.J. Tremolet de Villers, J.J. Berry, M.F. Van Hest, K. Zhu, ACS Energy Lett. 3 (2018) 322–328.
[22] L. Qiu, S. He, Z. Liu, L.K. Ono, D.-Y. Son, Y. Liu, G. Tong, Y. Qi, J. Mater. Chem. A 8 (2020) 23404–23412.
[23] Z. Yang, Z. Liu, V. Ahmadi, W. Chen, Y. Qi, Sol. RRL 6 (2022) 2100458.
[24] D.-K. Lee, N.-G. Park, Sol. RRL 6 (2022) 2100455.
[25] Y. Cheng, Y. Peng, A.-K.-Y. Jen, H.-L. Yip, Sol. RRL 6 (2022) 2100545.
[26] M. Xu, W. Ji, Y. Sheng, Y. Wu, H. Cheng, J. Meng, Z. Yan, J. Xu, A. Mei, Y. Hu, Nano Energy 74 (2020).
[27] X. Zhu, S. Yang, Y. Cao, L. Duan, M. Du, J. Feng, Y. Jiao, X. Jiang, Y. Sun, H. Wang, Adv. Energy Mater. 12 (2022) 2103491.
[28] J. Werner, C.C. Boyd, T. Moot, E.J. Wolf, R.M. France, S.A. Johnson, M.F. van Hest, J.M. Luther, K. Zhu, J.J. Berry, Energy Environ. Sci. 13 (2020) 3393–3403.
[29] L. Rakocevic, R. Gehlhaar, T. Merckx, W. Qiu, U.W. Paetzold, H. Fledderus, J. Poortmans, IEEE J. Photovolt. 7 (2016) 404–408.
[30] F. Fan, Y. Zhang, M. Hao, F. Xin, Z. Zhou, Y. Zhou, J. Energy Chem. 68 (2022) 797–810.
[31] C. Fei, B. Li, R. Zhang, H. Fu, J. Tian, G. Cao, Adv. Energy Mater. 7 (2017) 1602017.
[32] D. Wang, J. Zheng, X. Wang, J. Gao, W. Kong, C. Cheng, B. Xu, J. Energy Chem. 38 (2019) 207–213.
[33] F. Ye, H. Wang, W. Ke, C. Tao, G. Fang, J. Energy Chem. 73 (2022) 429–435.
[34] F. Huang, M. Li, P. Siffalovic, G. Cao, J. Tian, Energy Environ. Sci. 12 (2019) 518–549.
[35] Y. Vaynzof, Adv. Energy Mater. 10 (2020) 2003073.
[36] D. Li, D. Zhang, K.S. Lim, Y. Hu, Y. Rong, A. Mei, N.G. Park, H. Han, Adv. Funct. Mater. 31 (2021) 2008621.
[37] P. Du, L. Wang, J. Li, J. Luo, Y. Ma, J. Tang, T. Zhai, Adv. Opt. Mater. 10 (2022) 2101770.
[38] R. Swartwout, M.T. Hoerantner, V. Bulović, Energy Environ. Mater. 2 (2019) 119–145.
[39] M.R. Leyden, Y. Jiang, Y. Qi, J. Mater. Chem. A 4 (2016) 13125–13132.
[40] L. Qiu, S. He, Y. Jiang, D.-Y. Son, L.K. Ono, Z. Liu, T. Kim, T. Bouloumis, S. Kazaoui, Y. Qi, J. Mater. Chem. A 7 (2019) 6920–6929.
[41] T. Lei, F. Li, X. Zhu, H. Dong, Z. Niu, S. Ye, W. Zhao, J. Xi, B. Jiao, L. Ding, Sol. RRL 4 (2020) 2000292.
[42] J. Li, H. Wang, X.Y. Chin, H.A. Dewi, K. Vergeer, T.W. Goh, J.W.M. Lim, J.H. Lew, K.P. Loh, C. Soci, Joule 4 (2020) 1035–1053.
[43] D.B. Ritzer, T. Abzieher, A. Basibüyük, T. Feeney, F. Laufer, S. Ternes, B.S. Richards, S. Bergfeld, U.W. Paetzold, Prog. Photovoltaics Res. Appl. 30 (2022) 360–373.
[44] T. Bu, J. Li, F. Zheng, W. Chen, X. Wen, Z. Ku, Y. Peng, J. Zhong, Y.-B. Cheng, F. Huang, Nat. Commun. 9 (2018) 1–10.
[45] L. Qiu, Z. Liu, L.K. Ono, Y. Jiang, D.Y. Son, Z. Hawash, S. He, Y. Qi, Adv. Funct. Mater. 29 (2019) 1806779.
[46] E.H. Jung, N.J. Jeon, E.Y. Park, C.S. Moon, T.J. Shin, T.-Y. Yang, J.H. Noh, J. Seo, Nature 567 (2019) 511–515.
[47] A. Ren, H. Lai, X. Hao, Z. Tang, H. Xu, B.M.F.Y. Jeco, K. Watanabe, L. Wu, J. Zhang, M. Sugiyama, Joule 4 (2020) 1263–1277.
[48] S. Tian, J. Li, S. Li, T. Bu, Y. Mo, S. Wang, W. Li, F. Huang, Sol. Energy 183 (2019) 386–391.
[49] A. Agresti, S. Pescetelli, A.L. Palma, A.E. Del Rio Castillo, D. Konios, G. Kakavelakis, S. Razza, L. Cinà, E. Kymakis, F. Bonaccorso, ACS Energy Lett. 2 (2017) 279–287.
[50] A. Agresti, S. Pescetelli, A.L. Palma, B. Martín-García, L. Najafi, S. Bellani, I. Moreels, M. Prato, F. Bonaccorso, A. Di Carlo, ACS Energy Lett. 4 (2019) 1862–1871.
[51] T. Bu, X. Liu, J. Li, W. Huang, Z. Wu, F. Huang, Y.-B. Cheng, J. Zhong, Sol. RRL 4 (2020) 1900263.
[52] J.H. Heo, F. Zhang, C. Xiao, S.J. Heo, J.K. Park, J.J. Berry, K. Zhu, S.H. Im, Joule 5 (2021) 481–494.
[53] K.-S. Lim, D.-K. Lee, J.-W. Lee, N.-G. Park, J. Mater. Chem. A 8 (2020) 9345–9354.
[54] D.-K. Lee, K.-S. Lim, J.-W. Lee, N.-G. Park, J. Mater. Chem. A 9 (2021) 3018–3028.
[55] Z. Yang, W. Zhang, S. Wu, H. Zhu, Z. Liu, Z. Liu, Z. Jiang, R. Chen, J. Zhou, Q. Lu, X.W. Xiao, L. Shi, H. Chen, L.K. Ono, S.S. Zhang, Y.Q. Zhang, Y.B. Qi, L.Y. Han, W. Chen, Sci. Adv. 7 (2021) eabg3749.
[56] T. Bu, J. Li, H. Li, C. Tian, J. Su, G. Tong, L.K. Ono, C. Wang, Z. Lin, N. Chai, Science 372 (2021) 1327–1332.
[57] P.J.S. Rana, B. Febriansyah, T.M. Koh, B.T. Muhammad, T. Salim, T.J. Hooper, A. Kanwat, B. Ghosh, P. Kajal, J.H. Lew, Adv. Funct. Mater. 32 (2022) 2113026.
[58] Y. Deng, S. Xu, S. Chen, X. Xiao, J. Zhao, J. Huang, Nat. Energy 6 (2021) 633–641.
[59] R. Xue, M. Zhang, D. Luo, W. Chen, R. Zhu, Y.M. Yang, Y. Li, Y. Li, Sci. China Chem. 63 (2020) 987–996.
[60] J. Zhang, T. Bu, J. Li, H. Li, Y. Mo, Z. Wu, Y. Liu, X.-L. Zhang, Y.-B. Cheng, F. Huang, J. Mater. Chem. A 8 (2020) 8447–8454.
[61] L. Vesce, M. Stefanelli, J.P. Herterich, L.A. Castriotta, M. Kohlstädt, U. Würfel, A. Di Carlo, Sol. RRL 5 (2021) 2100073.
[62] L.A. Castriotta, F. Matteocci, L. Vesce, L. Cina, A. Agresti, S. Pescetelli, A. Ronconi, M. Löffler, M.M. Stylianakis, F. Di Giacomo, ACS Appl. Mater. Interfaces 13 (2021) 11741–11754.
[63] H. Li, T. Bu, J. Li, Z. Lin, J. Pan, Q. Li, X.-L. Zhang, Z. Ku, Y.-B. Cheng, F. Huang, ACS Appl. Mater. Interfaces 13 (2021) 18724–18732.
[64] Q. Feng, X. Huang, Z. Tang, Y. Hou, Q. Chang, S. Nie, F. Cao, X. Niu, J. Yin, J. Li, Energy Environ. Sci. 15 (2022) 4404–4413.
[65] H. Zeng, L. Li, F. Liu, M. Li, S. Zhang, X. Zheng, L. Luo, S. You, Y. Zhao, R. Guo, Adv. Energy Mater. 12 (2022) 2102820.
[66] S. Daskeviciute-Geguziene, Y. Zhang, K. Rakstys, G. Kreiza, S.B. Khan, H. Kanda, S. Paek, M. Daskeviciene, E. Kamarauskas, V. Jankauskas, Angew. Chem. Int. Ed. 61 (2022) e202113207.
[67] Y. Ding, B. Ding, H. Kanda, O.J. Usiobo, T. Gallet, Z. Yang, Y. Liu, H. Huang, J. Sheng, C. Liu, Nat. Nanotechnol. 17 (2022) 598–605.
[68] B. Ding, Y. Li, S.-Y. Huang, Q.-Q. Chu, C.-X. Li, C.-J. Li, G.-J. Yang, J. Mater. Chem. A 5 (2017) 6840–6848.

[69] X. Zhou, Y. Zhang, W. Kong, M. Hu, L. Zhang, C. Liu, X. Li, C. Pan, G. Yu, C. Cheng, J. Mater. Chem. A 6 (2018) 3012–3021.
[70] S. Paek, P. Schouwink, E.N. Athanasopoulou, K. Cho, G. Grancini, Y. Lee, Y. Zhang, F. Stellacci, M.K. Nazeeruddin, P. Gao, Chem. Mater. 29 (2017) 3490–3498.
[71] M. Remeika, Y. Qi, J. Energy Chem. 27 (2018) 1101–1110.
[72] L. Tao, J. Qiu, B. Sun, X. Wang, X. Ran, L. Song, W. Shi, Q. Zhong, P. Li, H. Zhang, J. Energy Chem. 61 (2021) 395–415.
[73] H. Yao, S. Shi, Z. Li, Z. Ci, G. Zhu, L. Ding, Z. Jin, J. Energy Chem. 57 (2021) 567–586.
[74] H. Si, Q. Liao, Z. Kang, Y. Ou, J. Meng, Y. Liu, Z. Zhang, Y. Zhang, Adv. Funct. Mater. 27 (2017) 1701804.
[75] Y. Bai, S. Xiao, C. Hu, T. Zhang, X. Meng, Q. Li, Y. Yang, K.S. Wong, H. Chen, S. Yang, Nano Energy 34 (2017) 58–68.
[76] L. Guo, Y. Chen, G. Wang, Y. Xia, D. Luo, Z. Zhu, C. Wang, W. Dong, S. Wen, A.C. S. Appl, Energy Mater. 4 (2021) 2681–2689.
[77] M. Vásquez-Montoya, J.F. Montoya, D. Ramirez, F. Jaramillo, J. Energy Chem. 57 (2021) 386–391.
[78] Y. Rong, S. Venkatesan, R. Guo, Y. Wang, J. Bao, W. Li, Z. Fan, Y. Yao, Nanoscale 8 (2016) 12892–12899.
[79] X. Guo, C. McCleese, C. Kolodziej, A.C. Samia, Y. Zhao, C. Burda, Dalton Trans. 45 (2016) 3806–3813.
[80] Y. Jo, K.S. Oh, M. Kim, K.H. Kim, H. Lee, C.W. Lee, D.S. Kim, Adv. Mater. Interfaces 3 (2016) 1500768.
[81] F. Yang, L. Dong, D. Jang, K.C. Tam, K. Zhang, N. Li, F. Guo, C. Li, C. Arrive, M. Bertrand, Adv. Energy Mater. 10 (2020) 2001869.
[82] M. Du, X. Zhu, L. Wang, H. Wang, J. Feng, X. Jiang, Y. Cao, Y. Sun, L. Duan, Y. Jiao, Adv. Mater. 32 (2020) 2004979.
[83] W. Xiang, J. Zhang, S.F. Liu, S. Albrecht, A. Hagfeldt, Z. Wang, Joule 6 (2022) 315–339.
[84] B. Martin, D. Amos, E. Brehob, M.F. van Hest, T. Druffel, Appl. Energy 307 (2022).
[85] B. Chen, C. Fei, S. Chen, H. Gu, X. Xiao, J. Huang, Nat. Commun. 12 (2021) 1–10.
[86] P. Zhao, B.J. Kim, X. Ren, D.G. Lee, G.J. Bang, J.B. Jeon, W.B. Kim, H.S. Jung, Adv. Mater. 30 (2018) 1802763.
[87] J. Xue, R. Wang, K.-L. Wang, Z.-K. Wang, I. Yavuz, Y. Wang, Y. Yang, X. Gao, T. Huang, S. Nuryyeva, J. Am. Chem. Soc. 141 (2019) 13948–13953.
[88] A. Kumar, S. Singh, M. Al-Bahrani, Surf. Interfaces 34 (2022).
[89] B. Gogoi, A. Yerramilli, K.M. Luboowa, E. Tagbor, T. Alford, J. Mater. Sci.: Mater. Electron. 33 (2022) 21161–21171.
[90] Q. An, L. Vieler, K.P. Goetz, O. Telschow, Y.J. Hofstetter, R. Buschbeck, A.D. Taylor, Y. Vaynzof, Adv. Energy Sustainability Res. 2 (2021) 2100061.
[91] J. Li, X. Hua, F. Gao, X. Ren, C. Zhang, Y. Han, Y. Li, B. Shi, S.F. Liu, J. Energy Chem. 66 (2022) 1–8.
[92] Y. Li, Z. Chen, B. Yu, S. Tan, Y. Cui, H. Wu, Y. Luo, J. Shi, D. Li, Q. Meng, Joule 6 (2022) 676–689.
[93] N. Ahn, D.-Y. Son, I.-H. Jang, S.M. Kang, M. Choi, N.-G. Park, J. Am. Chem. Soc. 137 (2015) 8696–8699.
[94] J.W. Lee, Z. Dai, C. Lee, H.M. Lee, T.H. Han, N. De Marco, O. Lin, C.S. Choi, B. Dunn, J. Koh, J. Am. Chem. Soc. 13 (2018) e0194422.
[95] G. Tong, D.Y. Son, L.K. Ono, Y. Liu, Y. Hu, H. Zhang, A. Jamshaid, L. Qiu, Z. Liu, Y. Qi, Adv. Energy Mater. 11 (2021) 2003712.
[96] Y. Tang, Z. Gu, C. Fu, Q. Xiao, S. Zhang, Y. Zhang, Y. Song, Sol. RRL 6 (2022) 2200120.
[97] C. Bi, Q. Wang, Y. Shao, Y. Yuan, Z. Xiao, J. Huang, Nat. Commun. 6 (2015) 1–7.
[98] Y. Shao, Y. Yuan, J. Huang, Nat. Energy 1 (2016) 1–6.
[99] X. Huang, G. Deng, S. Zhan, F. Cao, F. Cheng, J. Yin, J. Li, B. Wu, N. Zheng, A.C.S. Cent, Sci. 8 (2022) 1008–1016.
[100] J.E. Kim, S.S. Kim, C. Zuo, M. Gao, D. Vak, D.Y. Kim, Adv. Funct. Mater. 29 (2019) 1809194.
[101] X. Yu, J. Li, Y. Mo, T. Xiang, Z. Ku, F. Huang, F. Long, Y. Peng, Y.-B. Cheng, J. Energy Chem. 67 (2022) 201–208.
[102] F. Ma, Y. Zhao, J. Li, X. Zhang, H. Gu, J. You, J. Energy Chem. 52 (2021) 393–411.
[103] P. Mahajan, B. Padha, S. Verma, V. Gupta, R. Datt, W.C. Tsoi, S. Satapathi, S. Arya, J. Energy Chem. 68 (2022) 330–386.
[104] T. Guo, Z. Fang, Z. Zhang, Z. Deng, R. Zhao, J. Zhang, M. Shang, X. Liu, Z. Hu, Y. Zhu, J. Energy Chem. 69 (2022) 211–220.
[105] Q. Liu, J. Qiu, X. Yan, Y. Fei, Y. Qiang, Q. Chang, Y. Wei, X. Zhang, W. Tian, S. Jin, J. Energy Chem. 74 (2022) 387–393.
[106] Y. Deng, X. Zheng, Y. Bai, Q. Wang, J. Zhao, J. Huang, Nat. Energy 3 (2018) 560–566.
[107] C. Pereyra, H. Xie, M. Lira-Cantu, J. Energy Chem. 60 (2021) 599–634.
[108] J.-W. Lee, H.-S. Kim, N.-G. Park, Acc. Chem. Res. 49 (2016) 311–319.
[109] X. Cao, C. Li, L. Zhi, Y. Li, X. Cui, Y. Yao, L. Ci, J. Wei, J. Mater. Chem. A 5 (2017) 8416–8422.
[110] C. Yang, R. Zhi, M.U. Rothmann, F. Huang, Y.-B. Cheng, W. Li, Sol. RRL 6 (2022) 2100600.
[111] X. Li, D. Bi, C. Yi, J.-D. Décoppet, J. Luo, S.M. Zakeeruddin, A. Hagfeldt, M. Grätzel, Science 353 (2016) 58–62.
[112] S. Zhang, R. Guo, H. Zeng, Y. Zhao, X. Liu, S. You, M. Li, L. Luo, M. Lira-Cantu, L. Li, Energy Environ. Sci. 15 (2022) 244–253.
[113] F. Guo, S. Qiu, J. Hu, H. Wang, B. Cai, J. Li, X. Yuan, X. Liu, K. Forberich, C.J. Brabec, Adv. Sci. 6 (2019) 1901067.
[114] R. Chen, Y. Wang, S. Nie, H. Shen, Y. Hui, J. Peng, B. Wu, J. Yin, J. Li, N. Zheng, J. Am. Chem. Soc. 143 (2021) 10624–10632.
[115] L.-L. Gao, C.-X. Li, C.-J. Li, G.-J. Yang, J. Mater. Chem. A 5 (2017) 1548–1557.
[116] J. Ding, Q. Han, Q.-Q. Ge, D.-J. Xue, J.-Y. Ma, B.-Y. Zhao, Y.-X. Chen, J. Liu, D.B. Mitzi, J.-S. Hu, Joule 3 (2019) 402–416.
[117] D. Khim, H. Han, K.J. Baeg, J. Kim, S.W. Kwak, D.Y. Kim, Y.Y. Noh, Adv. Mater. 25 (2013) 4302–4308.
[118] K. Liu, Q. Liang, M. Qin, D. Shen, H. Yin, Z. Ren, Y. Zhang, H. Zhang, P.W. Fong, Z. Wu, Joule 4 (2020) 2404–2425.
[119] H. Hu, Z. Ren, P.W. Fong, M. Qin, D. Liu, D. Lei, X. Lu, G. Li, Adv. Funct. Mater. 29 (2019) 1900092.
[120] L.E. Mundt, L.T. Schelhas, Adv. Energy Mater. 10 (2020) 1903074.
[121] D.-K. Lee, D.-N. Jeong, T.K. Ahn, N.-G. Park, ACS Energy Lett. 4 (2019) 2393–2401.
[122] C.O. Teixeira, D. Castro, L. Andrade, A. Mendes, Energy Sci. Eng. 10 (2022) 1478–1525.
[123] M. Kim, G.-H. Kim, T.K. Lee, I.W. Choi, H.W. Choi, Y. Jo, Y.J. Yoon, J.W. Kim, J. Lee, D. Huh, Joule 3 (2019) 2179–2192.
[124] D.-H. Kang, Y.-J. Park, Y.-S. Jeon, N.-G. Park, J. Energy Chem. 67 (2022) 549–554.
[125] T. Bu, L.K. Ono, J. Li, J. Su, G. Tong, W. Zhang, Y. Liu, J. Zhang, J. Chang, S. Kazaoui, Nat. Energy 7 (2022) 528–536.
[126] Y. Deng, C.H. Van Brackle, X. Dai, J. Zhao, B. Chen, J. Huang, Sci. Adv. 5 (2019) eaax7537.
[127] B. Sun, W. Wang, H. Lu, L. Chao, H. Gu, L. Tao, J. Hu, B. Li, X. Zong, W. Shi, J. Phys. Chem. C 125 (2021) 6555–6563.
[128] K.H. Hendriks, J.J. van Franeker, B.J. Bruijnaers, J.A. Anta, M.M. Wienk, R.A. Janssen, J. Mater. Chem. A 5 (2017) 2346–2354.
[129] S. Chen, X. Dai, S. Xu, H. Jiao, L. Zhao, J. Huang, Science 373 (2021) 902–907.
[130] J.W. Yoo, J. Jang, U. Kim, Y. Lee, S.-G. Ji, E. Noh, S. Hong, M. Choi, S.I. Seok, Joule 5 (2021) 2420–2436.
[131] J. Dou, Q. Song, Y. Ma, H. Wang, G. Yuan, X. Wei, X. Niu, S. Ma, X. Yang, J. Dou, J. Energy Chem. 76 (2023) 288–294.
[132] L. Li, S. Zhang, Z. Yang, E.E.S. Berthold, W. Chen, J. Energy Chem. 27 (2018) 673–689.
[133] X. Dai, Y. Deng, C.H. Van Brackle, S. Chen, P.N. Rudd, X. Xiao, Y. Lin, B. Chen, J. Huang, Adv. Energy Mater. 10 (2020) 1903108.
[134] Y. Deng, Z. Ni, A.F. Palmstrom, J. Zhao, S. Xu, C.H. Van Brackle, X. Xiao, K. Zhu, J. Huang, Joule 4 (2020) 1949–1960.
[135] J. Yang, Y. Chen, W. Tang, S. Wang, Q. Ma, Y. Wu, N. Yuan, J. Ding, W.-H. Zhang, J. Energy Chem. 48 (2020) 217–225.
[136] Y. Niu, D. He, Z. Zhang, J. Zhu, T. Gavin, P. Falaras, L. Hu, J. Energy Chem. 68 (2022) 12–18.
[137] J. Ma, Z. Lin, X. Guo, L. Zhou, J. He, Z. Yang, J. Zhang, Y. Hao, S. Liu, J. Chang, J. Energy Chem. 63 (2021) 558–565.
[138] K. Jung, W.-S. Chae, J.W. Choi, K.C. Kim, M.-J. Lee, J. Energy Chem. 59 (2021) 755–762.
[139] J. Yang, J. Hu, W. Zhang, H. Han, Y. Chen, Y. Hu, J. Energy Chem. 77 (2023) 157–171.
[140] C. Fei, L. Guo, B. Li, R. Zhang, H. Fu, J. Tian, G. Cao, Nano Energy 27 (2016) 17–26.
[141] Y. Tu, J. Wu, X. He, P. Guo, H. Luo, Q. Liu, J. Lin, M. Huang, Y. Huang, L. Fan, Appl. Surf. Sci. 403 (2017) 572–577.
[142] J. Zhu, Y. Qian, Z. Li, O.Y. Gong, Z. An, Q. Liu, J.H. Choi, H. Guo, P.J. Yoo, D.H. Kim, Adv. Energy Mater. 12 (2022) 2200632.
[143] J. Li, H.-L. Cao, W.-B. Jiao, Q. Wang, M. Wei, I. Cantone, J. Lü, A. Abate, Nat. Commun. 11 (2020) 1–5.
[144] C. Liu, Y. Yang, K. Rakstys, A. Mahata, M. Franckevicius, E. Mosconi, R. Skackauskaite, B. Ding, K.G. Brooks, O.J. Usiobo, Nat. Commun. 12 (2021) 1–9.
[145] Y. Galagan, O. Open, Materials Science 1 (2021) itaa007.
[146] X. Tian, S.D. Stranks, F. You, Nat. Sustain. 4 (2021) 821–829.
[147] C. Ashworth, Nat. Rev. Mater. 6 (2021) 293.
[148] Z. Wang, Y. Lu, Z. Xu, J. Hu, Y. Chen, C. Zhang, Y. Wang, F. Guo, Y. Mai, Adv. Sci. 8 (2021) 2101856.
[149] B. Fan, J. Xiong, Y. Zhang, C. Gong, F. Li, X. Meng, X. Hu, Z. Yuan, F. Wang, Y. Chen, Adv. Mater. 34 (2022) 2201840.
[150] D. Jia, J. Chen, J. Qiu, H. Ma, M. Yu, J. Liu, X. Zhang, Joule 6 (2022) 1632–1653.
[151] O. Romiluyi, Y. Eatmon, R. Ni, B.P. Rand, P. Clancy, J. Mater. Chem. A 9 (2021) 13087–13099.
[152] L. Chao, T. Niu, W. Gao, C. Ran, L. Song, Y. Chen, W. Huang, Adv. Mater. 33 (2021) 2005410.
[153] P. Wang, X. Zhang, Y. Zhou, Q. Jiang, Q. Ye, Z. Chu, X. Li, X. Yang, Z. Yin, J. You, Nat. Commun. 9 (2018) 1–7.
[154] G. Wu, H. Li, J. Cui, Y. Zhang, S. Olthof, S. Chen, Z. Liu, D. Wang, S. Liu, Adv. Sci. 7 (2020) 1903250.
[155] E. Rezaee, W. Zhang, S.R.P. Silva, Small 17 (2021) 2008145.
[156] J. Wan, X. Yu, J. Zou, K. Li, L. Chen, Y. Peng, Y.-B. Cheng, Sol. Energy 226 (2021) 85–91.
[157] Z. Li, X. Wu, B. Li, S. Zhang, D. Gao, Y. Liu, X. Li, N. Zhang, X. Hu, C. Zhi, Adv. Energy Mater. 12 (2022) 2103236.
[158] A. Babayigit, A. Ethirajan, M. Muller, B. Conings, Nat. Mater. 15 (2016) 247–251.
[159] Y. Jiang, M. Remeika, Z. Hu, E.J. Juarez-Perez, L. Qiu, Z. Liu, T. Kim, L.K. Ono, D. Y. Son, Z. Hawash, Adv. Energy Mater. 9 (2019) 1803047.
[160] N.J. Jeon, J.H. Noh, Y.C. Kim, W.S. Yang, S. Ryu, S.I. Seok, Nat. Mater. 13 (2014) 897–903.
[161] X. Xiao, M. Wang, S. Chen, Y. Zhang, H. Gu, Y. Deng, G. Yang, C. Fei, B. Chen, Y. Lin, Sci. Adv. 7 (2021) eabi8249.

[162] E. Kesse-Guyot, D. Chaltiel, J. Wang, P. Pointereau, B. Langevin, B. Allès, P. Rebouillat, D. Lairon, R. Vidal, F. Mariotti, Nat. Sustain. 3 (2020) 377–385.
[163] N.-G. Park, Nat. Sustain. 4 (2021) 192–193.
[164] R. Vidal, J.-A. Alberola-Borràs, S.N. Habisreutinger, J.-L. Gimeno-Molina, D.T. Moore, T.H. Schloemer, I. Mora-Seró, J.J. Berry, J.M. Luther, Nat. Sustain. 4 (2021) 277–285.
[165] K.L. Gardner, J.G. Tait, T. Merckx, W. Qiu, U.W. Paetzold, L. Kootstra, M. Jaysankar, R. Gehlhaar, D. Cheyns, P. Heremans, Adv. Energy Mater. 6 (2016) 1600386.
[166] X. Zou, L. Zhou, W. Zhu, Y. Mao, L. Chen, J. neurosurgery 125 (2016) 746–753.
[167] W.S. Subhani, K. Wang, M. Du, X. Wang, N. Yuan, J. Ding, S.F. Liu, J. Energy Chem. 34 (2019) 12–19.
[168] B. Chen, J. Song, X. Dai, Y. Liu, P.N. Rudd, X. Hong, J. Huang, Adv. Mater. 31 (2019) 1902413.
[169] C. Musial, N. Knap, R. Zaucha, P. Bastian, G. Barone, G.L. Bosco, F. Lo-Celso, L. Konieczna, M. Belka, T. Bączek, Redox Biol. 55 (2022).

Zhaoyi Jiang obtained his B.S. in physics in 2012 from Shanxi Datong University, China, and his M.S. from Hebei University, China. He obtained his Ph.D. degree from Beihang University. He is currently a post-doctor at Huazhong University of Science and Technology. His research mainly focuses on large-area PSCs and modules.

Zhichun Yang received his B.S. in 2014 from Yun Cheng University, China, his M.S. in 2017, and his Ph.D. in 2021 from Huazhong University of Science and Technology, China. He is currently an associate professor at State Key Lab of Quantum Optics and Quantum Optics Devices, Institute of Laser Spectroscopy, Shanxi University, China. His research mainly focuses on semiconductor optoelectronic devices based on metal halide perovskites.

Zhiguo Zhao received his B.S. in 2007 from Tsinghua University, Beijing, and his Ph.D. in 2012 from the Institute of Chemistry, Chinese Academy of Science, Beijing. He is currently employed at Huaneng Clean Energy Research Institute as vice director of the Photovoltaic Technology Department, Principal Investigator in Perovskite Photovoltaics, Standing Director of the Renewable Technologies Subcommittee of IEEE PES Energy Development and Power Generation Satellite Committee, Member of the Photovoltaic Committee of China Renewable Energy Society. His research mainly focuses on renewable energy technologies, especially perovskite photovoltaics.

Zonghao Liu received his B.Sc. in 2011 and Ph.D. in 2016 from Huazhong University of Science and Technology (HUST), China. He was a visiting student at the University of California, Los Angeles, USA, in 2015. From 2016 to 2017, he was a research assistant at Peking University, China. From 2017–2019, he worked as a postdoctoral scholar at Okinawa Institute of Science and Technology Graduate University in Japan. He is an associate professor at Wuhan National Laboratory for Optoelectronics of HUST. His current research focuses on optoelectronics devices based on inorganic/organic perovskites, especially perovskite solar cells.

Wei Chen received his B.S. and Ph.D. degrees from the Materials Science and Engineering Department Tsinghua University. He worked as a Post-Doctoral Fellowship with the Department of Chemistry, Hong Kong University of Science and Technology, from 2008 to 2010. In addition, he was a Visiting Scholar with the National Institute for Materials Science, Japan, from 2014 to 2015. He is currently a professor with the Wuhan National Laboratory for Optoelectronics, Huazhong University of Science and Technology. His research interests cover synthesizing, understanding, and applications of functional nanomaterials and semiconductor thin films in next-generation solar cells, including PSCs.